Pressure and stress effects on the diffusion of B and Sb in Si and Si-Ge alloys

Michael J. Aziz* and Yuechao Zhao
Division of Engineering and Applied Sciences, Harvard University, Cambridge, Massachusetts 02138, USA

Hans-J. Gossmann
AMD, Hopewell Junction, New York 12533, USA

Salman Mitha† and Stephen P. Smith
Charles Evans and Associates, Sunnyvale, California 94086, USA

David Schiferl
Los Alamos National Laboratory, Los Alamos, New Mexico 87545, USA
(Received 9 September 2005; published 2 February 2006)

The hydrostatic pressure dependence of the diffusivity of B and Sb in Si and of B in $Si_{89}Ge_{11}$ has been measured. The diffusivity of Sb in Si is retarded by pressure, characterized by an apparent activation volume of $\tilde{V}_{Sb}=+0.06\pm0.04$ times the Si atomic volume Ω. The diffusivity of B is enhanced by pressure, characterized by an apparent activation volume of $\tilde{V}_B$ of (-0.16 ± 0.05) Ω. The diffusivity of B in strain-relaxed $Si_{89}Ge_{11}$ is imperceptibly pressure dependent, characterized by an apparent activation volume of $(+0.03\pm0.03)$ Ω. $\tilde{V}_B$ in Si is close to the activation volume for the interstitialcy mechanism calculated for B in Si by *ab initio* methods. $\tilde{V}_{Sb}$ is close to some values inferred from atomistic calculations for a vacancy mechanism; problems of interpretation are discussed. A phenomenological thermodynamic treatment of diffusion under hydrostatic and nonhydrostatic stress is developed for sample configurations in which virtually all point defect equilibration occurs at the free surface of a hydrostatically or biaxially strained thin film stack. Relationships are predicted between the effects of hydrostatic and biaxial stress on diffusion normal to the surface. The prediction for Sb diffusion agrees reasonably well with measured behavior for Sb diffusion in biaxially strained Si and Si-Ge films, lending additional support to the conclusion that the vacancy mechanism dominates Sb diffusion, and supporting the nonhydrostatic thermodynamic treatment. The same analysis is used to compare hydrostatic boron results with *ab initio* calculations and with literature values for the biaxial strain effect on diffusion, and the resulting agreements and disagreements are discussed critically. Predictions for the effect of biaxial strain on diffusion parallel to the surface are made using these results and analyses.

DOI: 10.1103/PhysRevB.73.054101 PACS number(s): 66.30.Jt, 61.72.Tt, 68.55.Ln, 85.40.Ry

I. INTRODUCTION

Because understanding and controlling diffusion-related phenomena have become increasingly important as semiconductor device dimensions decrease, diffusion in Si has been extensively studied. Despite this emphasis our understanding of the diffusion of many substitutional elements remains incomplete. A study of the dependence of the atomic diffusivity on pressure P and stress σ can provide valuable information to help elucidate atomistic diffusion mechanisms. Additionally, for band-gap engineering purposes, biaxial strain is designed into certain epitaxial semiconductor devices, e.g., heterojunction bipolar transistors for high-power and high-speed applications such as wireless communications. The study of stress effects on diffusion is an important part of the study of the stability of such strained-layer epitaxial materials. Furthermore, although bulk wafers cannot sustain significant nonhydrostatic stresses at diffusion temperatures, such stresses are sustained near interfaces with patterned films and in the films themselves. These stresses in integrated circuit materials and other multilayer devices can be quite large due to growth stresses, interfacial stresses, thermal expansion mismatch, or dislocations.[1] The complexities associated with nonhydrostatic stress states in these materials, as well as in initially biaxially strained materials after the breakdown of a smooth, flat film morphology, make the interpretation of stress effects in terms of basic mechanisms and the prediction of stress effects from known mechanisms quite difficult. However, in certain cases, hydrostatic pressure and simple nonhydrostatic stress states can provide sufficient information to permit the prediction of behavior under arbitrary stress states.[2,3]

In this paper, we report the diffusivities of B and Sb in Si and of B in $Si_{89}Ge_{11}$ measured under enhanced hydrostatic pressure. A thermodynamic treatment of diffusion in a film stack under nonhydrostatic stress in the absence of internal point defect sources is presented. The results are used to make predictions for the effect of biaxial strain on "vertical" diffusion (normal to the surface). Experimental results on diffusion under biaxial strain are reanalyzed and comparison is made with the predicted behavior. For Sb diffusion, we demonstrate consistency of the hydrostatic measurements with *ab initio* calculations for a vacancy mechanism and confirm a prediction of the nonhydrostatic thermodynamic treatment for the relationship between the effects of biaxial strain and hydrostatic strain on diffusion. For B diffusion, we dem-

onstrate consistency of our results with *ab initio* calculations for an interstitialcy mechanism and use the result, along with the biaxial strain effect measured by Kuo *et al.*,[4] as input to the nonhydrostatic thermodynamic diffusion analysis to predict the effect of biaxial strain on "lateral" diffusion (parallel to the surface).

The paper is organized as follows. In Sec. II we review and extend the thermodynamic treatment of diffusion under nonhydrostatic stress. In Sec. III we describe the experiment and in Sec. IV we present the experimental results for the effect of hydrostatic pressure on diffusion of Sb and B. In Sec. V we compare the results to theoretical values of the activation volume and reanalyzed results from the literature for vertical Sb and B diffusion under biaxial strain. We also make predictions for the effect of biaxial strain on lateral boron diffusion. In Sec. VI we present our conclusions.

II. PRESSURE AND STRESS EFFECTS ON DOPANT DIFFUSION

Because diffusion of substitutional elements in Si occurs by the superposition of the contributions from vacancy- (*V*-) and interstitial- (*I*-) mediated mechanisms, the diffusivity responds to variations in *I* and *V* concentrations induced by *P*, temperature *T*, and nonequilibrium point defect injection. When a solid is subjected to changes in *P* and *T*, the mobilities of all point defects are altered immediately. Additionally, the point defect concentrations quickly re-equilibrate at the surfaces and other point defect sources, if they exist; a growing diffusional zone of point defect re-equilibration then sweeps through the specimen from these sources. When the region sampled by experiments equilibrates rapidly with the sources compared to the experimental time scale, the measured diffusivity is the equilibrium value.

The equilibrium diffusivity[5,6] of dopant *A* under intrinsic doping conditions can be expressed as

$$D_A = \gamma_{AI} D_{AI} + (1 - \gamma_{AI}) D_{AV}, \tag{1}$$

where γ_{AI} is the interstitial-based fraction of diffusion, D_{AI} is the equilibrium diffusivity arising from the interstitial-based mechanism, and D_{AV} that arising from the vacancy mechanism of diffusion. A direct interchange mechanism is also plausible,[7] but we know of no evidence indicating that it is an important contributor to self-diffusion or dopant diffusion in Si.

The diffusivity of *A* by the *AX* mechanism (*X*=*I* or *V*) is given by

$$D_{AX}(\boldsymbol{\sigma}, T, x, C_A) = fga^2 \frac{C_{AX}(\boldsymbol{\sigma}, T, x, C_A)}{C_A} \Gamma_{AX}(\boldsymbol{\sigma}, T, x, C_A), \tag{2}$$

where *g* is a geometric factor (1/6 for a vacancy mechanism in most cubic structures), *a* is the jump distance, $\boldsymbol{\sigma}$ is the stress tensor, C_A is the dopant concentration, *x* is the alloy composition, *T* is the absolute temperature, Γ_{AX} is the jump rate of the *AX* complex that mediates diffusion, and *f* is the correlation factor. Let us consider C_{AX} and Γ_{AX} in turn, focusing on the effects of stress and temperature.

The equilibrium concentration of point defects under nonhydrostatic stress conditions has been shown[2] to depend on the stresses on all surfaces of the material, and to depend differently on the stress on the surface at which the point defects equilibrate than on the other stresses. The interaction of a formation strain tensor $\mathbf{V}^f$ with the stress tensor was shown to account for these dependencies. We focus here on thin films under biaxial strain and hydrostatic pressure in which virtually all point defect equilibration occurs at the "top surface of the wafer," i.e., the nearest surface to the atomic transport being measured, which we will take as normal to the $\hat{x}_3$ axis. Consider a thin film in a stack of films with coherent interfaces on top of a thick substrate. The film under consideration does not need to be the topmost film (i.e., the one in contact with vapor), as long as point defect equilibration in the film under consideration occurs by transport through intervening films to the top surface—the only crystal-fluid interface. In this case we can define a Gibbs free energy of point defect formation as

$$G^f = U^f - TS^f - \sigma_{ij} V^f_{ij}, \tag{3}$$

where U^f and S^f are the changes upon point defect formation of internal energy and local entropy (i.e., not counting the ideal entropy of mixing of defects on lattice sites) of the film, respectively. The formation strain tensor[2] $\mathbf{V}^f$-represents the dimension changes of the film upon point defect formation, which are conjugate to the macroscopic stress tensor $\boldsymbol{\sigma}$ applied externally (e.g., by coherency with a neighboring lattice-mismatched film). The sum over repeated Cartesian indices $i,j=1,2,3$ is implied throughout this paper. In general $\mathbf{V}^f$ is nonlocal: the dimension changes of the sample depend on where the point defect came from. The restriction of point defect equilibration to the top surface is sufficient for G^f to be a function of the instantaneous state of the system and not of the prior history of the sample's configuration, thereby permitting the treatment of G^f as a thermodynamic potential. For an (001) thin film geometry,

$$\mathbf{V}^f = \Omega \begin{bmatrix} 0 & & \\ & 0 & \\ & & \pm 1 \end{bmatrix} + \frac{V^r}{3} \begin{bmatrix} 1 & & \\ & 1 & \\ & & 1 \end{bmatrix}, \tag{4}$$

where Ω is the atomic volume. The plus sign is for vacancy formation and the minus sign is for interstitial formation throughout this paper. The first matrix, representing the dimension changes of the film upon lattice site formation or annihilation prior to relaxation, depends on where the point defects come from; because they are assumed to all come from the top surface the third diagonal element is the only nonzero element. Because $\mathbf{V}^f$ represents the macroscopic average over the formation of many point defects from many different sites on the top surface, the off-diagonal elements are zero by crystal symmetry although any particular configuration may have nonzero values. The second matrix represents the relaxation strain: the relaxation of the neighboring atoms to the newly made defect propagates out in all directions to the surfaces, resulting in a change in the volume of the crystal by an amount V^r. The scalar formation volume V^f is the trace of $\mathbf{V}^f$.

For substitutional dopant *A*, the concentration of mobile dopant-defect complexes *AX* is given by

$$C_{AX}(\boldsymbol{\sigma},T,x,C_A) = C_A \exp\frac{-1}{kT}[G^f_{AX}(\boldsymbol{\sigma},T,x,C_A)], \tag{5}$$

where k is Boltzmann's constant and G^f is the Gibbs free energy of formation of the AX defect; the dependence of G^f on C_A is due to the dependence on the Fermi level. The Arrhenius slope of C_{AX} is obtained by differentiating $\ln C_{AX}$ with respect to $(kT)^{-1}$, resulting in

$$-\frac{\partial \ln C_{AX}}{\partial\left(\frac{1}{kT}\right)_{\boldsymbol{\sigma},x,C_A}} = G^f - T\left(\frac{\partial G^f}{\partial T}\right)_{\boldsymbol{\sigma},x,C_A} \tag{6}$$

or, if we define the right-hand side as the enthalpy H^f of defect formation[8]

$$-\frac{\partial \ln C_{AX}}{\partial\left(\frac{1}{kT}\right)_{\boldsymbol{\sigma},x,C_A}} = H^f(\boldsymbol{\sigma},T,x,C_A). \tag{7}$$

From Eqs. (3) and (5) the dependence on stress[2] is given by the derivative of G^f with respect to σ_{ij} while T, x, C_A, and all independent components of the stress tensor are held constant:

$$-kT\frac{\partial \ln C_{AX}}{\partial \sigma_{ij}} = \frac{\partial U^f}{\partial \sigma_{ij}} - T\frac{\partial S^f}{\partial \sigma_{ij}} - \sigma_{ij}\frac{\partial V^f}{\partial \sigma_{ij}} - V^f_{ij}. \tag{8}$$

Although the Gibbs free energy of point defect formation in strained semiconductors contains contributions not just from mechanical work, but also from band bending and changes in Fermi level,[9] we show in Appendix A that the pressure derivative of the Gibbs free energy of formation is nevertheless simply the volume change of the crystal upon forming one point defect. Using the Gibbs relation for closed systems, expressed as a difference between internal energy changes of the film with and without an additional point defect[10]

$$dU^f = TdS^f + \sigma_{ij}dV^f_{ij}, \tag{9}$$

Eq. (8) reduces to

$$kT\frac{\partial \ln C_{AX}}{\partial \sigma_{ij}} = V^f_{ij}. \tag{10}$$

We next consider the jump rate $\Gamma(\boldsymbol{\sigma},T,x,C_A)$, which is obtained from transition state theory extended to nonhydrostatic stress states.[11] Consider a small region surrounding the migrating point defect, sufficiently large that changes in strain outside the region during the migration jump may be considered small. The small region is viewed as a thermodynamic subsystem in thermal and mechanical contact with a solid reservoir. In transition state theory[12] the subsystem undergoes a "chemical" change from the starting configuration AX to the critical saddle-point configuration AX^* in the atomic migration path, which has a different size and shape, by thermal fluctuation. The critical fluctuation is a member, whose probability can be computed, of an ensemble of configurations in equilibrium with the starting state. Nonhydrostatic stresses affect the probability of a critical fluctuation through mechanical work interactions with the shape changes of the subsystem. This same change from AX to AX^* may be brought about by an agent external to the subsystem and reservoir performing mechanical work R on the system, at constant temperature and macroscopic (far-field) stress. The jump rate depends on $R_{\min}$, the minimum (and, consequently, reversible) work required[13]

$$\Gamma(\boldsymbol{\sigma},T,x,C_A) = \nu \exp\frac{-R_{\min}(\boldsymbol{\sigma},T,x,C_A)}{kT}, \tag{11}$$

where ν is an attempt frequency,[12] assumed constant. For hydrostatic pressure $R_{\min}$ is the Gibbs free energy of migration and is independent of jump direction for crystallographically equivalent jumps. We are concerned with net transport along a particular macroscopic direction (e.g., [001]) and assume that all jumps contribute the same displacement in the direction of net transport. One can go beyond this assumption using the approach of Daw *et al.*[14] Nonhydrostatic stress may reduce the $R_{\min}$ of some migration jumps relative to that of others. We focus on the jump, or set of jumps, with the lowest free energy of migration that have a nonzero component along the direction of macroscopic transport.

We require expressions for the Arrhenius slope and stress derivative of $\ln \Gamma$. We determine the appropriate partial derivatives of $R_{\min}$ using Rice's thermodynamic formalism[15] for solids with internal variables such as the position of a dislocation or, in our case, the shape change of the subsystem during the fluctuation from AX to AX^*. The internal variables are[11] the deformation gradient $e^{\text{sub}}_{ij} \equiv \partial u_j/\partial x_i$, where $\mathbf{u}(\mathbf{x})$ is the displacement field, and the stresses on the boundaries of the subsystem $T^{\text{sub}}_{ij}(\sigma_{ij}, e^{\text{sub}}_{ij})$, where the first Piola-Kirchhoff stress $\mathbf{T}$ is the ratio of actual force to original, undeformed area. The σ_{ij} are the far-field stresses in the reservoir, resulting from the exterior boundary conditions on the reservoir, which has initial volume V^{mac}_0. The far-field strains in the reservoir are ε_{ij}. $R_{\min}$ is obtained from the product of the forces and the displacements on the boundaries of the subsystem during the transition $AX \rightarrow AX^*$:

$$R_{\min}(\sigma_{ij},T,x,C_{\text{A}}) = V^{\text{sub}}_0 \int_{AX}^{AX^*} T^{\text{sub}}_{ij}(\sigma_{ij}, e^{\text{sub}}_{ij}, T, x, C_{\text{A}}) de^{\text{sub}}_{ij}, \tag{12}$$

where V^{sub}_0 is the volume of the subsystem in the starting state, and the path is any reversible path. The Arrhenius slope of $\ln \Gamma$ is determined from Eq. (11) by

$$-\frac{\partial \ln \Gamma}{\partial(1/kT)} = R_{\min} - T\frac{\partial R_{\min}}{\partial T} \tag{13}$$

and the stress derivative by

$$-kT\frac{\partial \ln \Gamma}{\partial \sigma_{ij}} = \frac{\partial R_{\min}(\sigma_{ij},T,x,C_{\text{A}})}{\partial \sigma_{ij}}. \tag{14}$$

Rice's generalized Helmholtz free energy, which includes work from the internal variables, is defined by

$$d\Phi = V^{\text{mac}}_0 \sigma_{ij} d\varepsilon_{ij} + V^{\text{sub}}_0 T^{\text{sub}}_{ij} de^{\text{sub}}_{ij} - SdT \tag{15}$$

and its dual potential on strain $\Psi \equiv \Phi - V^{\text{mac}}_0 \sigma_{ij}\varepsilon_{ij}$, gives

$$d\Psi = -V_0^{\mathrm{mac}}\varepsilon_{ij}d\sigma_{ij} + V_0^{\mathrm{sub}}T_{ij}^{\mathrm{sub}}de_{ij}^{\mathrm{sub}} - SdT. \tag{16}$$

From Eq. (15) follows the Maxwell relation

$$V_0^{\mathrm{sub}}\frac{\partial T_{ij}^{\mathrm{sub}}}{\partial T} = -\frac{\partial S}{\partial e_{ij}^{\mathrm{sub}}} \tag{17}$$

which, when substituted with Eq. (12) into Eq. (13), yields

$$-\frac{\partial \ln \Gamma}{\partial(1/kT)} = R_{\min} + TS^m, \tag{18}$$

with the migration entropy S^m being the change in entropy of the system upon being taken reversibly from AX to AX^* at constant T and σ_{ij} by the external agent.

As defined, $R_{\min}$ is always path independent for a given pair of end points. We therefore define the Gibbs free energy of point defect migration G^m under nonhydrostatic stress as

$$G^m = R_{\min}(\sigma_{ij}, T, x, C_{\mathrm{A}}). \tag{19}$$

Further, we define the migration enthalpy H^m as $R_{\min}+TS^m$. From Eq. (16) follows the Maxwell relation

$$V_0^{\mathrm{sub}}\frac{\partial T_{ij}^{\mathrm{sub}}}{\partial \sigma_{ij}} = -V_0^{\mathrm{mac}}\frac{\partial \varepsilon_{ij}}{\partial e_{ij}^{\mathrm{sub}}} \tag{20}$$

which, when substituted with Eq. (12) into Eq. (14), yields the migration strain tensor $\mathbf{V}^m$

$$kT\frac{\partial \ln \Gamma}{\partial \sigma_{ij}} = V_{ij}^m, \tag{21}$$

where $V_{ij}^m \equiv V_0^{\mathrm{mac}}\int_{AX}^{AX^*} d\varepsilon_{ij}$.

For diffusion in an (001)-oriented wafer we expect the macroscopic behavior to be characterized by a diffusivity in the [001] direction D_{33} with a migration strain tensor $\mathbf{V}_{33}^m$ with symmetry

$$\mathbf{V}_{33}^m = \begin{bmatrix} V_\perp^m & & \\ & V_\perp^m & \\ & & V_\parallel^m \end{bmatrix}, \tag{22}$$

and a diffusivity in the (100) direction D_{11} with a migration strain tensor $\mathbf{V}_{11}^m$ with symmetry

$$\mathbf{V}_{11}^m = \begin{bmatrix} V_\parallel^m & & \\ & V_\perp^m & \\ & & V_\perp^m \end{bmatrix}. \tag{23}$$

The scalar migration volume V^m is the trace of $\mathbf{V}^m$.

The overall behavior of D_{33} is thus given by

$$D_{33}(\boldsymbol{\sigma}, T, x, C_A) = fga^2\nu \exp\frac{-1}{kT}[G^f(\boldsymbol{\sigma}, T, x, C_A) + G^m(\boldsymbol{\sigma}, T, x, C_A)], \tag{24}$$

where we have dropped the subscript AX on D, G^f, and G^m for convenience. The dependence of the correlation factor[16–19] on $\boldsymbol{\sigma}$, T, x, and C_A is generally unknown. Commonly f is assumed to be constant, as it must be for self-diffusion in pure elements. There is some disagreement among treatments of the T dependence for impurities. Analogous approaches for the dependence on pressure or stress are evident.

Our approach, chosen for generality, permits f to be any smooth function of temperature and stress. We do not advance a model for this dependence but develop a treatment that can accommodate any model.[20] We define an apparent Gibbs free energy of activation $\tilde{G}$ by

$$D_{33} \equiv ga^2\nu_0 e^{-(\tilde{G}_{33}/kT)}, \tag{25}$$

so that

$$\tilde{G}_{33} = G^f + G^m - kT\ln\frac{f\nu}{\nu_0}, \tag{26}$$

where ν_0 is the attempt frequency under standard conditions. The apparent Gibbs free energy of activation contains both the "true" free energy of activation $G^* \equiv G^f + G^m$ and the preexponential factors that depend on ambient conditions.[21] The apparent activation enthalpy $\tilde{H}$ is the Arrhenius slope

$$\tilde{H}_{33} \equiv -\frac{\partial \ln D_{33}(\boldsymbol{\sigma}, T, x, C_A)}{\partial\left(\frac{1}{kT}\right)} = H^f + H^m - \frac{\partial \ln f(\boldsymbol{\sigma}, T, x, C_A)\nu(\boldsymbol{\sigma}, T, x, C_A)}{\partial\left(\frac{1}{kT}\right)}, \tag{27}$$

where the "true" activation enthalpy is $H^* = H^f + H^m$. Although the quantity $\mathbf{V}_{33}^* = \mathbf{V}^f + \mathbf{V}_{33}^m$ might, analogously, be called the "true" activation strain, the stress derivatives of $\ln D_{33}$ give the elements of the "apparent" activation strain $\tilde{\mathbf{V}}_{33}$:

$$\tilde{V}_{33,ij} \equiv kT\frac{\partial \ln D_{33}(\boldsymbol{\sigma}, T, x, C_A)}{\partial \sigma_{ij}} = V_{ij}^f + \tilde{V}_{33,ij}^m, \tag{28}$$

where

$$\tilde{V}_{33,ij}^m \equiv V_{33,ij}^m + kT\frac{\partial \ln f(\boldsymbol{\sigma}, T, x, C_A)\nu(\boldsymbol{\sigma}, T, x, C_A)}{\partial \sigma_{ij}}. \tag{29}$$

We expect $\tilde{\mathbf{V}}_{33}^m$ to have the same symmetries as $\mathbf{V}_{33}^m$, Eq. (22). We see no profound reason why either of these quantities is more "true" than the other: $\mathbf{V}_{33}^m$ might more appropriately be termed the "simple" migration strain and $\tilde{\mathbf{V}}_{33}^m$ the "effective" migration strain. Likewise for D_{11} there is a $\tilde{\mathbf{V}}_{11}^m$ with the same symmetries as $\mathbf{V}_{11}^m$ in Eq. (23). Using Eqs. (4) and (22), Eq. (28) can be written

$$\tilde{\mathbf{V}}_{33} = \Omega\begin{bmatrix} 0 & & \\ & 0 & \\ & & \pm 1 \end{bmatrix} + \frac{V^r}{3}\begin{bmatrix} 1 & & \\ & 1 & \\ & & 1 \end{bmatrix} + \begin{bmatrix} \tilde{V}_\perp^m & & \\ & \tilde{V}_\perp^m & \\ & & \tilde{V}_\parallel^m \end{bmatrix}. \tag{30}$$

In the above discussion we have assumed a single dominant mechanism for simplicity. When several mechanisms provide significant contributions in parallel, contributions from each mechanism would be superposed by combining

one equation such as Eq. (24) for each mechanism into an equation such as Eq. (1). Under these circumstances, even if the correlation factor is constant, the result of an experimental series that measures the dependence of D_{33} on temperature or stress is interpreted as an apparent activation enthalpy or activation strain arising from the weighted contributions of the operant mechanisms.

For cubic crystals under hydrostatic pressure, Eq. (28) reduces to[22]

$$\tilde{V} \equiv -kT\frac{\partial \ln D(P,T,x,C_A)}{\partial P} = V^* - kT\frac{\partial \ln f(P,T,x,C_A)\nu(P,T,x,C_A)}{\partial P}, \quad (31)$$

where D becomes a scalar, the (scalar) "apparent" activation volume $\tilde{V}$ is the trace of Eq. (30), the (scalar) "true" activation volume V^* is the trace of the "true" activation strain, the sum of Eqs. (4) and (22). There are several experimental determinations of $\tilde{V}$ and theoretical determinations of V^* for diffusion in Si.

There is substantial evidence that Sb diffusion is almost solely vacancy mediated. Gossmann *et al.*[6] determined experimentally that $\gamma_{SbI}(790\ ^\circ\mathrm{C}) \leqslant 0.01 \pm 0.01$. For solely vacancy-mediated diffusion $V^*_{Sb} = V^*_{SbV} = V^f_{SbV} + V^m_{SbV} = (V^f_V + V^{asso}_{SbV}) + V^m_{SbV} = (+\Omega + V^r_V) + V^{asso}_{SbV} + V^m_{SbV}$, where the formation volume V^f_{SbV} is the volume change of the system upon formation of a Sb-V pair by creating a vacancy at a kink site on a step on the surface and bringing it next to a preexisting Sb; the migration volume V^m_{SbV} is the additional volume change when the Sb-V pair reaches the saddle point in its migration path; V^f_V is the formation volume of an isolated vacancy, which is the sum of Ω and the relaxation volume V^r_V; and the pairing volume V^{asso}_{SbV} is the volume change upon association of a Sb-V pair from a widely separated Sb and V. Several of these volume changes for V-based mechanisms have been predicted by quantum-mechanical atomistic calculations.[23–25] The difference between V^*_{Sb} and $\tilde{V}_{Sb}$, arising from the potential of a pressure-dependent correlation factor as in Eq. (31), has not been modeled theoretically: the difference has generally been assumed to be zero.

Although different experiments for B diffusion over the years have been the subject of greatly conflicting interpretations regarding the relative contributions from vacancy and interstitial-based mechanisms,[26] the more recent evidence supports a nearly 100% interstitial-based mechanism in Si and in alloys up to 20% Ge.[6,27–30] For solely interstitialcy-mediated diffusion, $V^*_B = V^*_{BI} = V^f_{BI} + V^m_{BI} = (V^f_I + V^{asso}_{BI}) + V^m_{BI} = (-\Omega + V^r_I) + V^{asso}_{BI} + V^m_{BI}$, where the formation volume V^f_{BI} is the volume change of the system upon formation of a B-I pair; the migration volume V^m_{BI} is the additional volume change when the B-I pair reaches the saddle point in its migration path; V^f_I is the formation volume of an isolated Si self-interstitial, which is the sum of $-\Omega$ and the relaxation volume V^r_I; and the pairing volume V^{asso}_{BI} is the volume change $(V^{asso}_{BI} = V^f_{BI} - V^f_I)$ upon association of a B-I pair from a widely separated B and I. Several of these terms for proposed boron diffusion mechanisms have been investigated by atomistic calculations of the energetics[29,30] and, more recently, the volumetrics[29,31] of point defect formation and migration. As for Sb, the difference between V^*_B and $\tilde{V}_B$ has generally been assumed to be zero.

There have been several experimental studies of dopant diffusion in biaxially strained heteroepitaxial semiconductors.[4,9,32–38] The nonhydrostatic thermodynamic treatment developed above provides a framework for the interpretation of such experiments.

The elements V^r, $\tilde{V}^m_\perp$, and $\tilde{V}^m_\parallel$ in Eq. (30) are all, in principle, dependent on $\boldsymbol{\sigma}$, T, x, and C_A. We generally expect, though we are not guaranteed, that for small stresses (compared to, say, the biaxial modulus of 180 GPa for Si; i.e., for small strains), these volumes are nearly independent of stress, permitting us to use only the first term of a Taylor expansion of $\ln D_{33}$ in powers of stress. The resulting expression (treating T, x, and C_A as constants),

$$\frac{D_{33}(\boldsymbol{\sigma})}{D_{33}(\mathbf{0})} = \exp\frac{\sum_{i,j=1}^{3} \sigma_{ij}\tilde{V}_{33,ij}}{kT}, \quad (32)$$

should be checked against experimental data for signs of systematic deviations. According to Eqs. (30) and (32), hydrostatic pressure then influences D_{33} according to

$$\frac{D_{33}(P)}{D_{33}(0)} = \exp\left(\frac{-P[\pm\Omega + V^r + \tilde{V}^m]}{kT}\right), \quad (33)$$

where the apparent activation volume is $\tilde{V} = V^f + \tilde{V}^m$ or

$$\tilde{V} = \pm\Omega + V^r + \tilde{V}^m. \quad (34)$$

Biaxial tension in the x_1-x_2 plane with magnitude σ_{biax} influences D_{33} according to

$$\frac{D_{33}(\sigma_{biax})}{D_{33}(0)} = \exp\left(\frac{\sigma_{biax}\frac{2}{3}[V^r + \tilde{V}^m - \tilde{A}\Omega]}{kT}\right), \quad (35)$$

where

$$\tilde{A} \equiv \frac{(\tilde{V}^m_\parallel - \tilde{V}^m_\perp)}{\Omega} \quad (36)$$

is the anisotropy (normalized to Ω) in the effective migration volume or strain.

Experimentally, the influence of biaxial stress has been commonly[33,34] characterized by Q', defined by

$$\frac{D_{33}(\varepsilon_{biax},T,x,C_A)}{D_{33}(0,T,x,C_A)} = \exp -\left(\frac{Q'}{kT}\varepsilon_{biax}\right) \quad (37)$$

and termed the *apparent* change in activation energy E^* with biaxial strain ε_{biax}. As defined by these authors, Q' does not reflect solely the strain-dependence of E^*; it also reflects the strain dependence of the activation entropy. By comparison with Eq. (25) it may be thought of as the strain derivative of the apparent Gibbs free energy of activation. Comparison of Eqs. (35) and (37) permits the identification of Q' as a combination of volume changes upon point defect formation and migration:

$$Q' = -\frac{2}{3} Y[V^r + \tilde{V}^m - \tilde{A}\Omega], \tag{38}$$

where Y is the biaxial modulus of the film. Additionally, Eqs. (34) and (38) lead to the prediction

$$\frac{\tilde{V}}{\Omega} + \frac{3}{2}\frac{Q'}{Y\Omega} = \pm 1 + \tilde{A}. \tag{39}$$

If the anisotropy is negligible then the right-hand side (RHS) of Eq. (39) should be +1 for a vacancy mechanism and −1 for an interstitial-based mechanism.[39] Furthermore, in some cases it has been argued that the anisotropy in the true migration strain $A \equiv (V_{\parallel}^m - V_{\perp}^m)/\Omega$ is necessarily zero due to crystal symmetry.[2,14] The general problem remains unsolved of which crystal symmetries in ground state, saddle point, and direction of motion are sufficient to require $A=0$, and the conditions for $\tilde{A}=0$ are entirely unexplored.

According to this phenomenological nonhydrostatic thermodynamic treatment, for any given point defect mechanism, knowledge of the three parameters V^r, $\tilde{V}_{\parallel}^m$, and $\tilde{V}_{\perp}^m$ in Eq. (30) should permit the prediction of the effect of arbitrary stress states on D_{33}. These parameters could be determined experimentally by measuring diffusion under a variety of uniform stress states. The parameters can also determined theoretically by molecular statics or dynamics calculations if the stress dependence of the correlation factor can be modeled accurately or safely assumed to be negligible.

We have discussed how, in the presence of multiple mechanisms, contributions from each must be superposed. This applies also if there are multiple species or charge states for what is normally considered a single "mechanism." Additionally, strain breaks the energetic degeneracy of otherwise symmetry-equivalent ground states as well as saddle configurations; in principle, they must all be enumerated and superposed.[40] Determining the phenomenological parameters from the tensorial dilatations associated with an individual point defect ground-state and saddle-point configuration can be a significant problem in combinatorics.[14] In effect, the treatment presented above averages over the otherwise symmetry-equivalent configurations. The precise boundaries of its domain of validity are unknown, but averaging is expected to be reasonable if the degeneracy splitting $\ll$kT. At diffusion temperatures ~800 °C this condition readily satisfied; it is equivalent to an upper limit of $\sim 8\Omega$ on the magnitude of elements of $\mathbf{V}^*$ for films under $\leqslant 1\%$ biaxial strain as are those considered in this work. Furthermore, in a crystal structure whose primitive cell has a multiple-atom basis such as Si, each site in the basis set must be tracked separately.[14] This complication is unnecessary for diffusion along $\langle 100 \rangle$ directions in an (001) wafer under uniform hydrostatic or biaxial stress, as both sites in the two-atom basis are then equivalent.

We seek a confluence of theory and experiment not only to enhance confidence in the mechanism, but ultimately to permit predictions of the effect of an arbitrary stress state on diffusion in an arbitrary direction. Within the regime of validity of Eq. (30), for predicting diffusion along any cube axis (D_{11}, D_{22}, or D_{33}, the latter perpendicular to the wafer surface) under arbitrary stress states the three parameters occur in only two independent combinations, e.g.,

$$\frac{D_{33}(\boldsymbol{\sigma})}{D_{33}(\mathbf{0})} = \text{function of}\left[\left(\frac{V^r}{3} + \tilde{V}_{\parallel}^m\right), \left(\frac{V^r}{3} + \tilde{V}_{\perp}^m\right)\right]. \tag{40}$$

This means that for diffusion by mechanisms for which the apparent migration strain anisotropy $\tilde{A}$ is zero ($\tilde{V}_{\parallel}^m = \tilde{V}_{\perp}^m$), the result from a measurement under a single stress state should, in principle, permit the prediction of D_{11}, D_{22}, or D_{33} under arbitrary stress states (although it cannot uniquely separate V^r from $\tilde{V}_m$). And for diffusion by mechanisms for which $\tilde{A} \neq 0$, the results from only two independent measurements are required, in principle, to permit the prediction of the effect of an arbitrary stress state. More generally, for a given mechanism, all of the information about the phenomenological activation strain tensor is contained within the stress-strain work term of lattice site creation[2] during point defect formation, and the local configuration change in creation of the defect at the saddle configuration. The strain tensor for this latter change has at most six independent elements.[14]

III. EXPERIMENT

In the present study we used B and Sb doping superlattices (DSLs) in Si(001) fabricated by low T molecular beam epitaxy (MBE) growth[41,42] on float-zone substrates and single 20-nm-thick B-doped layers of unstrained $Si_{89}Ge_{11}$ and Si grown by chemical vapor deposition (CVD) on thick buffer layers on Czochralski substrates.[4] The Sb DSLs contain six equally spaced ~10 nm wide Sb-rich layers spaced 100 nm apart with peak concentrations of 6×10^{19} atoms/cm^3. The first spike is at 50 nm depth. The B DSLs contain six equally spaced ~10-nm-wide B-rich layers spaced 100-nm apart with peak concentrations of 2×10^{19} atoms/cm^3. The first spike is at 70 nm depth. Diffusion in the MBE-grown samples in vacuum and in Ar at atmospheric P has been characterized.[42] The CVD-grown B-doped $Si_{89}Ge_{11}$ and Si samples were left over from the experiments reported by Kuo *et al.* in Ref. 4; their diffusion behavior in Ar at atmospheric P was characterized in that work. The peak boron concentration is $\sim 1 \times 10^{18}$ atoms/cm^3 and $\sim 3 \times 10^{18}$/cm^3 at ~7 and ~10 nm depth for the alloy and Si samples, respectively.

All bulk, as-grown samples were thinned mechanically from the back side to ~35 μm thickness. After thinning, both front and back sides of the samples were cleaned using the standard RCA method[43] leaving a clean ~2-nm-thick SiO_2 layer on the surface. To prevent ambient effects on diffusion,[44] a Si_3N_4/SiO_2 surface passivation layer was produced by immediately depositing a 12-nm-thick Si_3N_4 layer on the freshly cleaned samples using argon-nitrogen dual-beam sputtering with the sample temperature remaining below 180 °C.[45]

High P anneals were performed in a high-T, high-P diamond-anvil cell (DAC) using fluid argon as the inert, clean, hydrostatic pressure transmitting medium. Argon (0.99998) was passed through a hot Ti gettering furnace. P in the DAC was measured[46] using the P-induced wavelength

shift of Sm:YAG fluorescence. Prior to heating, the furnace was evacuated and then filled with helium gas of nominal purity 99.995% to a gauge pressure of 260 Torr above atmospheric. The He ambient provides a homogenous temperature field around the DAC and minimizes oxidation of the contents of the furnace. Pressure in the DAC can be controlled from outside the furnace without disturbing the vacuum or the overpressure state in the furnace. The temperature was controlled using a programmable Eurotherm 818 temperature controller. Three thermocouples recorded T. One slides into a hole bored into the upper plate of the DAC, one slides into a hole bored into the lower plate, and the third is suspended between the plates. The variation among these thermocouple readings was within 3 °C; the reported T value is taken as their average value. The thermocouples were calibrated using the 1 bar melting points of Pb (328 °C), Sb (631 °C), GaSb (710 °C), NaCl (810 °C), and Ag (961 °C), permitting an absolute calibration within ±10 °C and a run-to-run reproducibility of 2 °C.

B and Sb concentration-depth profiles were measured using secondary ion mass spectrometry (SIMS) on a Cameca 4F magnetic sector instrument with an 8 keV primary O_2^+ ion beam at ~39° from normal incidence. The detected species were $^{11}B^+$ and $^{123}Sb^+$, empirically determined for best signal to noise. The raster area was about 100–150 microns. To reduce artificial broadening due to the "crater wall effect," the raster size was greater than the lateral dimensions of the samples. The depth scale was determined from features in the elemental depth profile. Both electronic and physical gating were used. The accepted area was about a 30 micron circle with electronic gating being used to cut off stray particles that come from the optical aberrations resulting from the sample edges. In Fig. 1 we show typical SIMS concentration-depth profiles for B and Sb DSL samples.

Values for diffusivity were determined using the process simulator PROPHET by evolving the measured initial profile numerically according to[42]

$$\frac{\partial C_A}{\partial t} = \frac{\partial}{\partial z}\left(D_A \frac{\partial C_A}{\partial z}\right), \tag{41}$$

where A=B or Sb, and finding the best fit to the measured final profile. Under extrinsic doping conditions, which is the case for our samples, the extrinsic diffusivities for B and Sb are expressed as[5,47–49]

$$D_A = \left(\frac{hD_A^{\text{int}}}{1+\beta}\right)\left(1+\frac{\beta m}{n_i}\right), \tag{42}$$

where m is the electron concentration for A=Sb and the hole concentration for A=B; n_i is the pressure- and composition-dependent intrinsic carrier concentration and h is the electric field enhancement factor, which varies from 1 to 2 as doping conditions vary from intrinsic to extrinsic. In the case of B (Sb) diffusion, β is the ratio of the contributions to diffusion from positively (negatively) charged and neutral interstitials (vacancies). We have assumed[50] that these contributions have the same activation volume resulting in a P-independent β. To estimate n_i in the pressurized $Si_{1-x}Ge_x$ alloys, we have scaled the value of n_i in pure Si using the relation

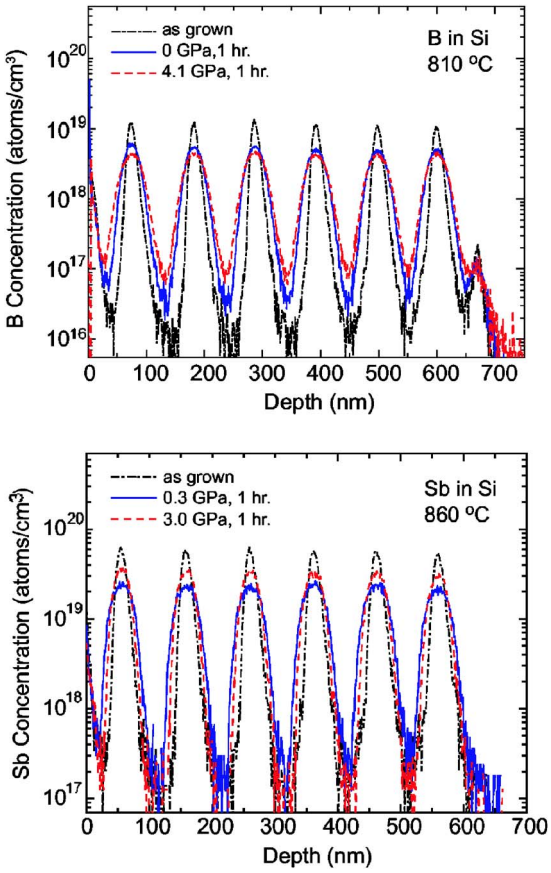

FIG. 1. (Color online) Typical SIMS concentration-depth profiles for MBE-grown (top) boron-doped and (bottom) Sb-doped Si samples. Hydrostatic pressure accelerates B diffusion and retards Sb diffusion.

$$n_i(x,P) = [n_i(0,0)][(1-x)\sqrt{N_c^{\text{Si}}N_v^{\text{Si}}} + x\sqrt{N_c^{\text{Ge}}N_v^{\text{Ge}}}]\exp\left(\frac{\alpha_x x}{2k_BT}\right)\exp\left(\frac{\alpha_P P}{2k_BT}\right), \tag{43}$$

where the N_c's and N_v's are the effective densities of states at the conduction and valence band edges, respectively, in the pure elements at zero pressure, α_x=0.290 eV,[51] and α_P =−24.5 meV/GPa[52] and is assumed independent of x, consistent with common observations in semiconductors.[53]

IV. RESULTS

A. Sb diffusion

In Fig. 2 we show the P dependence of the time-averaged intrinsic Sb diffusivity at 860 °C for 1 h anneals. Our measured values, extrapolated to 1 atm, are consistent with the values of $4–5\times10^{-17}$ cm^2/s obtained from previous measurements with 1 atm. Ar as the annealing ambient.[54]

The average of the slopes of the fitted curves is $\tilde{V}$ =+0.06 Ω. The final value of the uncertainty in $\tilde{V}$ requires the inclusion of additional uncertainties from the various components of the experiment,[55] resulting in $\tilde{V}$ =(−0.06±0.04) Ω.

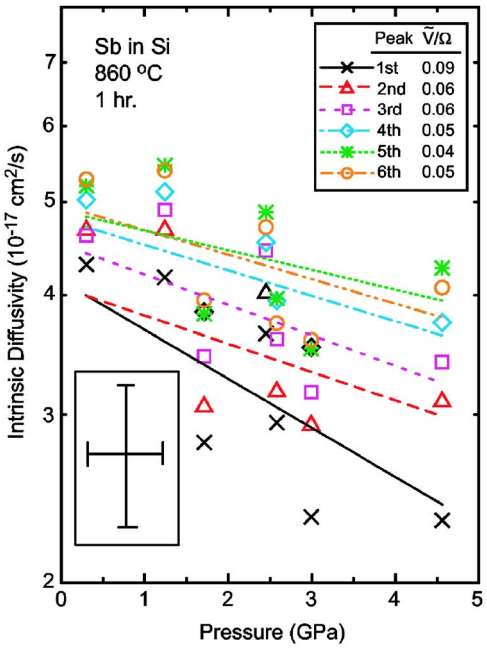

FIG. 2. (Color online) Intrinsic Sb diffusivity for each of six MBE-grown doping spikes vs pressure at 860 °C. Typical error bars for data points are shown in inset on left. Apparent activation volumes calculated from best fit slopes are shown in upper right.

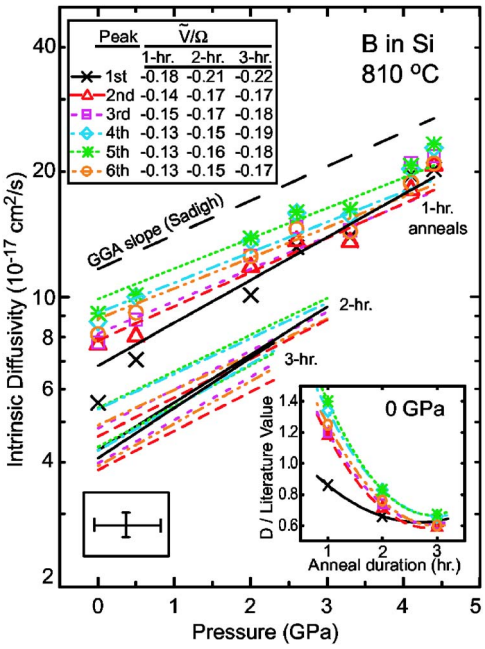

FIG. 3. (Color online) Intrinsic B diffusivity for each of six MBE-grown doping spikes vs pressure at 810 °C. Activation volumes calculated from best-fit slopes are shown in upper left. As two-hour anneals were performed only once at 0 and 3.0 GPa, and three-hour anneals were performed only once at 0 and 2.3 GPa, the end points of the fitted lines identify the locations of the data points, which are not explicitly plotted. Inset, left: typical error bars for data points. Inset, right: 0 GPa data replotted vs time with curves to guide the eye; anomalous first spike is lowest curve. The rate of decay for spikes 2–6 appears to be the same at high P as at 0 GPa. Dashed line: slope corresponding to $\tilde{V}/\Omega=-0.15$ (offset arbitrary) predicted by *ab initio* (GGA) calculations ($T=0$) of Sadigh *et al.* with hexagonal boron interstitial saddle point assuming pressure-independent correlation factor. Other theoretically-derived values are in Table II.

The nature of the uncharacteristic behavior of the first spike, at 50 nm depth, which had been observed previously for these samples[54] and the B-doping superlattice samples (discussed later) is not understood. The measured effective diffusivities of vacancies[54] and interstitials are, respectively, 5×10^{-11} and 1×10^{-11} cm^2/s in these samples[56]; these values yield diffusion time constants of 1.2 and 6.0 min, respectively, for vacancies and interstitials to traverse the top 600 nm region containing the Sb spikes. Therefore we expect that $\tilde{V}$ measured on the 1 h anneals is truly characteristic of equilibrium conditions. This expectation is consistent with the lack of a time dependence observed by Mogi *et al.*[54] in samples grown simultaneously with ours.

B. Boron diffusion

In Fig. 3 we show the P dependence of the time-averaged intrinsic boron diffusivity of the boron DSLs at 810 °C over 1–3 h anneals. The activation volumes for the individual spikes are reported in units of Ω. The nature of the uncharacteristic behavior of the first spike (at 70 nm depth) and the transient behavior for all spikes is not understood; the latter may be related to the out-diffusion or recombination with self-interstitials of $\sim3\times10^{14}$/cm^3 excess grown-in vacancies[42,57] or to precipitation of $\sim10^{18}$/cm^3 dissolved oxygen.[58] The decrease of D_B with time, shown explicitly in the inset, is consistent with the measured[48] effective self-interstitial diffusivity of $D_I=1.5\times10^{-12}$ cm^2/s in these samples; this value yields a diffusion time of 40 min for penetration of the diffusional boundary layer from the surface to the bottom spike. We expect therefore that $\tilde{V}$ measured on the longer anneals is truly characteristic of equilibrium point defect concentrations. With the exception of the first spike, all $\tilde{V}$ values lie in the range (-0.16 ± 0.03) Ω. Therefore our measurement of $\tilde{V}$ using spikes 2–6 is not subject to the nuances of the interpretation of the origin of the time dependence.[59] The best-fit value of $\tilde{V}$ averaged over six spikes and three anneal durations for all the spikes is −0.16 Ω. The final value of the uncertainty in $\tilde{V}$ requires the inclusion of additional uncertainties from the various components of the experiment,[60] resulting in $\tilde{V}=(-0.16\pm0.05)$ Ω.

B diffusion in Si has been studied by *ab initio* theoretical calculations,[29–31,61] all of which are restricted to $T=0$. The most recent calculations[29–31] indicate an interstitialcy mechanism with several competing paths. When the Fermi level is at or slightly below midgap the predominant saddle point is predicted to be neutral interstitial boron close to a hexagonal (ring-center) site; the predominant ground state is predicted to be a BI^+ pair with boron occupying a lattice site bonded to four lattice neighbors and a self-interstitial in a neighboring tetrahedral interstice. When the Fermi level is closer to the valence band edge than to midgap, calculations using the

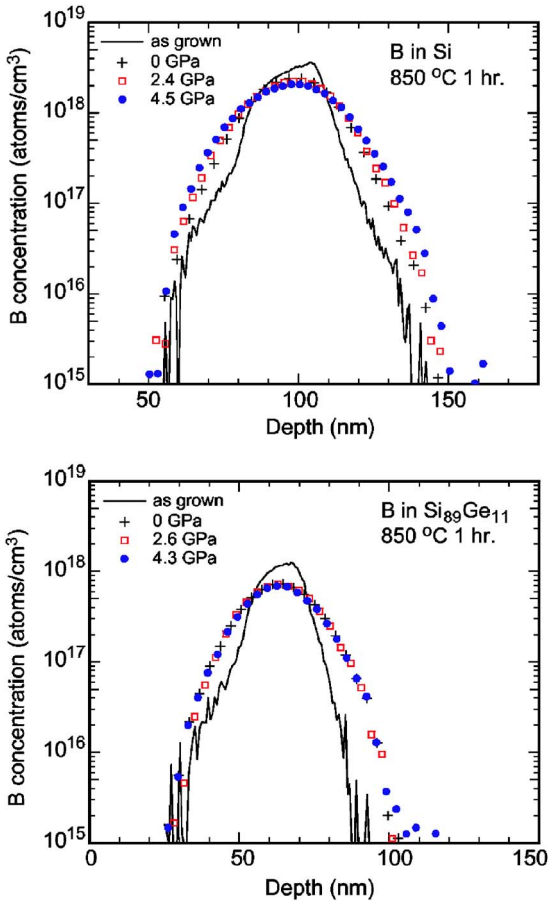

FIG. 4. (Color online) SIMS boron concentration-depth profiles for CVD-grown (a) Si and (b) $Si_{89}Ge_{11}$ samples annealed under hydrostatic pressure. Unalloyed samples show pressure-enhanced diffusivity characterized by $\tilde{V}=-(0.16\pm0.05)\ \Omega$; alloys show $\tilde{V}$ indistinguishable from zero.

generalized gradient approximation (GGA), but not those using the local density approximation (LDA), indicate that the charge state of the saddle configuration switches to singly positive.[30] Although the peak concentration in each of our dopant profiles is in this regime, we ignore the possible charge state switch between profile peak and profile tail due to lack of consensus; lack of sufficient information about the positively charged saddle configuration (which has not been studied as thoroughly as the neutral saddle configuration) and the observation that the importance of the diffusion pathway with the neutral hexagonal interstitial saddle point is enhanced by entropic factors.[30]

In Fig. 4 we show typical SIMS concentration-depth profiles for the CVD-grown single doping-layer Si and $Si_{89}Ge_{11}$ samples annealed for 1 h at 850 °C. We have ignored some "surface" boron found at <50 nm depth in the unalloyed sample, which may be due to surface segregation or contamination, and have analyzed only the shape of the buried spike centered at 70–100 nm. The results are presented in Table I. The absolute magnitude of the intrinsic diffusivity at 0 GPa is significantly below that reported by Kuo *et al.* We believe the most likely origin of the discrepancy is our deposition of a nitride surface passivation layer onto the native oxide on

TABLE I. Intrinsic boron diffusivity measured in this work on Kuo's CVD-grown layers of Si on Si and $Si_{89}Ge_{11}$ on $Si_{89}Ge_{11}$. All anneals were in argon for 1 h at 850 °C in diamond-anvil cell after nitride capping as described in text.

x_{Ge}, fraction Ge	P (GPa)	D_{33}^{int} (10^{-17} cm^2/s)
0	0	5.9±1.4
0	2.4	11.2±1.4
0	4.5	15.2±1.4
0.11	0	9.8±0.9
0.11	2.6	8.7±1.1
0.11	4.3	8.3±1.5

Kuo's samples, which may have changed the surface boundary condition on the point defect populations. Additionally, it is possible that the temperature calibrations, SIMS depth-profiling techniques, methods of profile fitting and extraction of the intrinsic diffusivity might have been rather different in our work than in that of Kuo *et al.* For an interpretation not subject to such possible systematic errors, we compare our data only to themselves. Best-fit simulated final profiles (not shown in Fig. 4) indicate a pressure-enhanced diffusivity in the Si. The activation volume resulting from the fitting of these profiles in the unalloyed sample is $\tilde{V}=(-0.16\pm0.05)\ \Omega$, in remarkable agreement with the results from the boron DSLs. In marked contrast to the observed behavior in Si, as shown in the bottom panel of Fig. 4, the activation volume for the unstrained $Si_{89}Ge_{11}$ alloy is indistinguishable from zero: $\tilde{V}=(-0.03\pm0.03)\ \Omega$. The results of the hydrostatic pressure experiments, the predictions of density functional theory, and the resulting predictions for biaxial strain using Eq. (39) are compiled in Table II.

V. DISCUSSION

A. Comparison to theoretical values of V^*

For Sb in Si, Table III summarizes the experimental and theoretical results. Sugino and Oshiyama[25] (SO) performed an LDA calculation of Sb diffusion by a vacancy mechanism assuming a migration pathway in which, after interchanging with the dopant, the vacancy circumnavigates a hexagonal ring to approach the dopant from a different direction, thereby permitting long-range transport. They found that the saddle point in the migration path was at the third nearest-neighbor position (3NN), i.e., diagonally opposite the impurity, and reported a change in activation energy of −0.7 eV at 6 GPa pressure. This change does not include the $+P\Omega$ lattice site formation term in the work of vacancy formation and hence we interpret it to indicate $V^*-\Omega=-0.934\ \Omega$, implying $V^*=+0.066\ \Omega$. Likewise, we interpret SO's calculations for the isolated Si vacancy as indicating a formation volume of $V_V^f=+0.468\ \Omega$. There have been more recent *ab initio* calculations of formation volumes for the Si vacancy that disagree with the SO result. Antonelli, Kaxiras, and Chadi[24] found two vacancy configurations very close in en-

TABLE II. Boron diffusion under hydrostatic stress. Experimental and theoretical hydrostatic pressure effects on diffusion in Si and $Si_{89}Ge_{11}$; implications using Eq. (39) assuming interstitialcy mechanism.

Measurement and calculation, hydrostatic stress	No. of D data points	x_{Ge}	T (°C)	$\tilde{V}/\Omega$	Q' (eV) if $\tilde{A}=0$
$D_{33}^{int}(P)$ data, MBE Si	10×6	0	810	-0.16 ± 0.05	-11.6 ± 0.7
$D_{33}^{int}(P)$ data, CVD Si	3	0	850	-0.16 ± 0.05	-11.6 ± 0.7
$D_{33}^{int}(P)$ data, CVD $Si_{89}Ge_{11}$	3	0.11	850	-0.03 ± 0.03	-13.2 ± 0.40
GGA Si (Windl)		0	−273	$V^*/\Omega=-0.26$	−10.2
GGA Si (Sadigh)		0	−273	$V^*/\Omega=-0.15$	−11.8
LDA Si (Sadigh)		0	−273	$V^*/\Omega=-0.11$	−12.3

ergy with very large inward relaxation around the vacancy core; the formation volume for the smaller of the two configurations (the predominant configuration under pressure) is $-0.086\ \Omega$. Windl *et al.*[62] used both the LDA and the GGA, examined supercell sizes containing up to 1000 atoms, and concluded $V_V^f=(-0.10\pm0.06)\ \Omega$. Zhao *et al.*[63] have recently used the GGA to obtain $V_V^f=-0.083\ \Omega$, which is consistent with the more recent calculations but not with SO; they have also calculated V^* for Sb diffusion by the vacancy ring circumnavigation mechanism. They found that if the saddle point configuration is the 3NN position then V^* is $+0.02\ \Omega$, which is very close to both the experimental result of $\tilde{V}=(0.06\pm0.04)\ \Omega$ reported here and the SO result for V^*. However, they found a slightly higher saddle point between the second-neighbor and third-neighbor positions with a different volume. They found that if this is the effective saddle point for migration, as is commonly believed,[18,64] then $V^*=-0.21\ \Omega$, which differs significantly from the measured value of $\tilde{V}$. The apparent discrepancy between this calculated value for V^* and the measured value of $\tilde{V}$ may be due to a pressure-dependent correlation factor. Recently Ramanarayanan *et al.*[19] found from kinetic Monte Carlo (KMC) simulations of Ge diffusion in Si by a vacancy mechanism that the temperature dependence does not correspond to any particular energy barrier in the migration path, thereby showing that the correlation factor varies significantly with T. In light of this finding, a pressure-dependent f must also be considered plausible.

We regard the comparison between calculated V^* and measured $\tilde{V}$ as unsettled. The apparent discrepancy between the latest theoretical value and experiment is small enough that it could be due to errors in calculation or measurement at this stage. The discrepancy between KMC simulations and simple models for the temperature dependence of Ge diffusion in Si is a concern whose resolution may have to await future work. For example, it is important to see whether the correlation factor is significantly T dependent for charged dopants, which are expected to have a longer-range attraction for charged vacancies than does Ge. Additionally, the discrepancy among the *ab initio* calculations remains a nagging concern. It may be related to the difference between the P dependence of the enthalpy of formation and that of the Gibbs free energy of formation. SO imposed a unit cell volume, thereby imposing a P, and calculated the resulting change in point defect energy; combined with the $P\Omega$ work of lattice site creation this procedure yields essentially the P dependence of the enthalpy of formation. The others permitted the lattice parameters to relax at constant P; combined with the volume change upon lattice site creation this procedure directly yields the formation volume, which is the P dependence of the Gibbs free energy of formation. The difference between these two quantities is the P dependence of the entropy of formation, which has not been evaluated; it could be evaluated directly[7,65] or, via a Maxwell relation, determined from the temperature dependence of the formation volume.

For B in Si, with a supercell constrained to remain equiaxed, Sadigh *et al.*[29] determined $V^*=-0.11\ \Omega$ for the LDA and $-0.15\ \Omega$ for the GGA. In a fully nonhydrostatic calculation, Windl and co-workers[30,31] determined $V^*=-0.26\ \Omega$ using GGA. The better consistency among these theoretical

TABLE III. Theoretical and measured volume changes (in units of Ω) associated with Sb diffusion in Si. Values for the right-hand column are obtained by subtracting V_V^f from V^*. Bold values have been determined directly (either experimentally or theoretically); other values result from our interpretation.

Work	V^*	V_V^f	$V^{asso}+V_{SbV}^m$
Sugino and Oshiyama	+0.066	−0.468	+0.534
This experiment	$\tilde{V}/\Omega=+0.06\pm0.04$		
Antonelli, Kaxiras, and Chadi		−0.09	
Windl *et al.*		-0.10 ± 0.06	
Zhao *et al.*:		−0.08	
third neighbor position	+0.02		+0.10
2-3 saddle	−0.21		−0.13

results compared to those for the vacancy formation volume may be associated with the observation of Windl *et al.*[62] that convergence with supercell size is much faster for interstitial-based than for vacancy-based configurations. It is encouraging that our measured value of $\tilde{V}=-0.16\ \Omega$ is bracketed by these theoretical results. The slope predicted from the median of these three values of V^*, assuming f is constant, is plotted above the data as a dashed line in Fig. 3. Although it is by no means guaranteed that f is constant, the consistency is encouraging.

B. Comparison to Sb diffusion under biaxial strain

We compare our results for Sb with the measured effect of biaxial stress on diffusion using Eq. (39). In the simplest case of a vacancy mechanism in which the saddle point has a symmetry axis along the direction of the elementary atomic jumps $\langle 111\rangle$ for D_{33} the migration volume anisotropy A is zero. This occurs because compression along all $\langle 100\rangle$ directions necessarily changes the energy of this saddle point the same amount. Whereas this condition should clearly be satisfied for the vacancy contribution to self-diffusion, if dopant diffusion proceeds via a higher and more important effective saddle point at or near the 3NN position[17,18,25,64] to the dopant atom, i.e., the symmetry axis of the saddle point could be along or near the $\langle 311\rangle$ direction pointing from the dopant to the vacant 3NN site. In these cases it remains to be determined whether the broken symmetry causes $\tilde{A}$ to have a magnitude of any significance. Because the elementary jumps of the impurity atom remain in $\langle 111\rangle$ directions, all of which are symmetrically equivalent to stress along any given $\langle 100\rangle$ direction, we expect $A=0$ independent of the magnitude of the degeneracy splitting between saddle points even if the latter have $\langle 311\rangle$ symmetry axes.

Experimentally, Kringhoj *et al.*[34] were the first to isolate the effects of strain and composition on Sb diffusion normal to the surface. They measured the diffusivity of Sb in $Si_{1-x}Ge_x$ films coherently strained between substrates and capping layers of $Si_{1-y}Ge_y$. They reported $Q'=13\pm3$ eV per unit strain for compressively strained alloy ($x=0.09$) films on Si ($y=0$), and $Q'=17\pm5$ eV for tensile Si ($x=0$) films on the alloy ($y=0.09$) over the temperature range 900–1025 °C. The composition of these alloy films was subsequently determined to be $x=8\%$ Ge, and the diffusivity measurements extended to higher alloy compositions and to temperatures as low as 815 °C.[36,66] Focusing on the dilute alloys, we have collected "the Aarhus data" by taking the reported $D(T,x,y)$ data points[67] tabulated in Ref. 36 and digitized the nontabulated data from the available plots.[34,36,68] Kringhoj and Nylandsted Larsen[35] also reported the curiously low value of $Q'(6\pm3$ eV) for $x=0.11$ alloys under biaxial tension, but no data are reported that might permit a further analysis.

Motivated by Eqs. (24)–(28), focusing on the intrinsic diffusivity so C_A is no longer an independent variable, Taylor expanding $\tilde{G}_{33}(\boldsymbol{\sigma},T,x)$ about $(0,T_0,0)$, and substituting $Y\varepsilon_{\rm biax}$ for $\sigma_{\rm biax}$, we obtain

$$\ln D_{33}^{\rm int}=\ln D_0^{\rm int}-\frac{1}{kT}\tilde{H}_{33}(0,T_0,0)-\frac{\varepsilon_{biax}}{kT}Q'(0,T_0,0)-\frac{x}{kT}Q'_x(0,T_0,0), \tag{44}$$

where $Q'_x\equiv\partial\tilde{G}_{33}/\partial x$ and $D_0^{\rm int}=ga^2\nu\exp[\tilde{S}_{33}(0,T_0,0)/k]$ with $\tilde{S}_{33}\equiv-\partial\tilde{G}_{33}/\partial T$. A linear regression of $\ln D_{33}$ against[69] $-1/kT$, $-\varepsilon_{\rm biax}/kT$, and $-x/kT$, performed according to Eq. (44) for the 26 unique data points with $x=0$, 0.08, and 0.10 obtained from the Aarhus data, yields $D_0=10^{(+0.95\pm0.22)}$ cm^2/s, corresponding to $\tilde{S}_{33}/k=9.2\pm9.7$ at 925 °C (assuming $\nu=10^{13}$ Hz); $Q'=(16.6\pm1.4)$ eV per unit strain; an apparent activation enthalpy of $\tilde{H}_{33}=(4.00\pm0.05)$ eV; and a composition derivative of the apparent free energy of activation of $Q'_x=(0.948\pm0.083)$ eV per unit composition. Elastic constants, lattice parameters, and the corresponding strains and stresses were determined as shown in Appendixes B and C. Regression results for those constant-composition subsets of the data on which regressions are possible, and their implications, are shown in Table IV. No significant composition dependence of the fitting parameters is evident for the composition range covered ($0\leqslant x\leqslant0.10$). Additionally, no significant temperature dependence of the fitting parameters was found. The comparison of the fitted values of Q' with the result of our hydrostatic pressure experiment $\tilde{V}=+0.06\ \Omega$ using Eq. (39), is shown in Table IV. The hydrostatic data series (this work) shows our measured value of $\tilde{V}/\Omega$ in the sixth column and, in the fifth column, the value for Q' required by Eq. (39) assuming a vacancy mechanism and $\tilde{A}=0$. For the biaxial data series, the sixth column is the value of $\tilde{V}/\Omega$ required by Eq. (39) using the values of Q' from the regressions and assuming a vacancy mechanism with $\tilde{A}=0$. The seventh column is the required value of $\tilde{V}/\Omega$ assuming an interstitial-based mechanism and $\tilde{A}=0$; the enormous difference from our measured value of V^* is apparent. Alternatively, one can combine the hydrostatic and biaxial diffusion results to obtain an experimental "measurement" of the apparent migration strain anisotropy necessary to exactly reconcile the two data sets through Eq. (39). The eighth and ninth columns are required values of $\tilde{A}$ for vacancy and interstitial-based mechanisms, respectively, if $\tilde{V}$ for each of these alloys is the value measured by us for unalloyed Si. The values for the vacancy mechanism are small and plausible, and the values for the interstitial-based mechanism are implausibly large.

Considering only the eleven data points for unalloyed Si, against which our hydrostatic measurements should be most directly comparable, we find $Q'=(16.8\pm2.1)$ eV per unit strain. We find $\tilde{V}+(3/2)(Q'/Y)=(+1.29\pm0.19)\ \Omega$ for unalloyed Si. This is in reasonably good agreement with the prediction of $+1\ \Omega$ for a simple vacancy mechanism $\tilde{A}=0$, especially compared to the prediction of $-1\ \Omega$ expected for an interstitial-based mechanism. The combination of hydrostatic and biaxial results indicates that an anisotropy $\tilde{A}$

TABLE IV. Antimony diffusion. Hydrostatic and biaxial strain effects on diffusion in Si and $Si_{1-x}Ge_x$; implications using Eq. (39). Bold values have been determined directly; other values result from our interpretation. Hydrostatic data series (this work) shows measured value of $\tilde{V}/\Omega$ in the sixth column and, in the fifth column, required value for Q' assuming a vacancy mechanism and zero apparent migration strain anisotropy. Biaxial data series show Q' values determined by us in a linear regression of reported diffusivities to Eq. (44). The sixth column is the required value of $\tilde{V}/\Omega$ assuming a vacancy mechanism and zero apparent migration strain anisotropy. The seventh column is the required value of $\tilde{V}/\Omega$ assuming an interstitial-based mechanism and zero apparent migration strain anisotropy. The eighth and ninth columns are required values of anisotropy for vacancy and interstitial-based mechanisms, respectively, if $\tilde{V}$ for each of these alloys is the value measured by us for unalloyed Si.

Hydrostatic data series	No. of data points	x_{Ge}	T(°C)	Q'(eV) if $\tilde{A}=0$ and vacancy mechanism	$\tilde{V}/\Omega$			
Hydrostatic $D_{33}^{int}(P)$ data, MBE Si	7×6	0	860	12.9±0.5	0.06±0.04			
Biaxial $D_{33}(\varepsilon_{biax})$ data series, MBE Si and $Si_{1-x}Ge_x$	**No. of data points**	x_{Ge}	Avg. T(°C)	Q'(eV)	$\tilde{V}/\Omega$ if $\tilde{A}=0$ and vacancy mechanism	$\tilde{V}/\Omega$ if $\tilde{A}=0$ and interstitial mechanism	$\tilde{A}$ if vacancy mechanism and $\tilde{V}/\Omega$ =+0.06±0.04	$\tilde{A}$ if interstitial mechanism and $\tilde{V}/\Omega$ =+0.06±0.04
Aarhus $x=0$	11	0	950	16.8±2.1	−0.23±0.16	−2.23±0.16	0.29±0.19	2.29±0.19
Aarhus $x=0.08$	11	0.08	950	13.3±2.2	0.01±0.16	−1.99±0.16	0.05±0.20	2.05±0.20
Aarhus $0\leqslant x\leqslant 0.1$	26	0–0.10	925	16.6±1.4	−0.23±0.10	−2.23±0.10	0.28±0.14	2.30±0.14
Portavoce $x=0.09$	12	0.09	775	2.7±3.0	0.81±0.22	−1.19±0.22	−0.75±0.26	1.25±0.26
Portavoce $x=0.18$	12	0.18	750	12.5±3.0	0.08±0.22	−1.92±0.22	−0.02±0.26	1.98±0.26
Portavoce $x\leqslant 0.18$	37	0–0.18	780	5.8±1.9	0.58±0.14	−1.42±0.14	−0.52±0.18	1.48±0.18

$=0.29\pm0.19$ is required for a vacancy mechanism, and $\tilde{A}=2.29\pm0.19$ is required for an interstitial-based mechanism. The required anisotropy for a vacancy mechanism is close to zero but is more than one standard deviation away. This could reflect a stress-induced anisotropy in the correlation factor. It should be noted, however, that the reported uncertainties in the measured values of $\tilde{V}$ and Q' do not reflect possible systematic errors, which are difficult to evaluate. From our own experience, we suspect that systematic errors—especially in cross comparisons of two different experiments performed on different samples grown in different laboratories—could easily be as large as the quoted statistical uncertainties. Hence we consider our hydrostatic $\tilde{V}$ measurement, the Aarhus biaxial Q' measurement, the vacancy mechanism with zero or small apparent migration strain anisotropy, and the nonhydrostatic thermodynamic treatment to be mutually consistent. These results provide further evidence that Sb diffuses predominantly by a vacancy mechanism, and demonstrate progress toward predictive capability for the effect of nonhydrostatic stress on diffusion.

Recently, Portavoce *et al.* have made Sb diffusivity measurements[37,70] on an extensive series of strained alloys with compositions $x=0$, 0.03, 0.07, 0.09, 0.15, and 0.18, ranging over somewhat lower temperatures (700–850 °C) than the Aarhus data. We performed a linear regression of Eq. (44) for the 37 data points in this study.[71] The result is $D_0=10^{(-0.60\pm0.63)}$ cm^2/s, corresponding to $\tilde{S}_{33}/k=5.6\pm1.5$ at 780 °C, $\tilde{H}_{33}=(3.5\pm1.4)$ eV, $Q'=(5.8\pm1.9)$ eV per unit strain, and $Q'^{x}=(0.94\pm0.13)$ eV per unit composition. This data set has somewhat more scatter than the Aarhus data ($R^2=0.954$ for the Portavoce data vs $R^2=0.997$ for the Aarhus data). Two compositions $x=0.09$ and $x=0.18$ were studied sufficiently thoroughly that the effect of strain at constant x and T may be ascertained directly, as shown in Fig. 5. Curiously, the strain effect appears much weaker for the $x=0.09$ alloys ($Q'=2.7\pm3.0$ eV per unit strain) than for the $x=0.18$ alloys ($Q'=12.5\pm3.0$ eV). A regression of the Aarhus data for $x=0$, 0.08, and 0.10 to Eq. (44) has been used to predict $D_{33}(\varepsilon_{biax})$ for $x=0.09$, $T=850$ °C; the result is the long dashed line in Fig. 5. That this line lies well below the data of Portavoce *et al.* for this composition and temperature reflects the lower dopant concentration in the Aarhus samples. The solid line indicates the slope predicted for 850 °C from $\tilde{V}=+0.06$ Ω and Eq. (39) for a vacancy mechanism with $\tilde{A}=0$. The agreement of both lines is quite satisfactory with the observed strain effect on the high-composition Portavoce alloys but not the low-composition alloys. Although the difference in experimental temperature ranges between the Aarhus data and the Portavoce data admits the possibility of a temperature dependence to Q', this would not explain the difference between the Portavoce $x=0.09$ alloys and the Portavoce $x=0.18$ alloys. There are reports of Sb clusters in the SiGe alloys[70] and perhaps their presence has affected the reported value of D in a manner slightly differently than anticipated in the data analysis. These results and their implications for volumetrics and

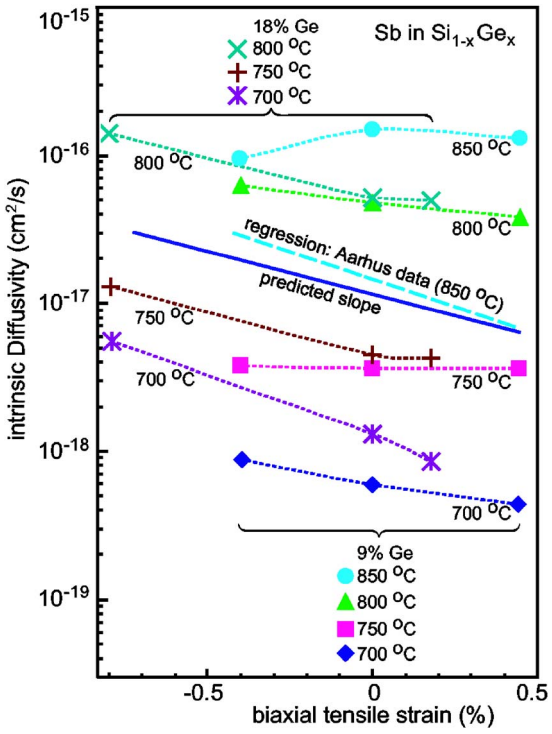

FIG. 5. (Color online) Strain effect on Sb diffusion in $Si_{1-x}Ge_x$ at constant x and T; data from Portavoce *et al.* Data series spanning strain range −0.4–+0.45 % and identified by filled symbols are for $x=0.09$; series spanning range −0.8–+0.2 % and identified by unfilled symbols are for $x=0.18$. Dotted lines are to guide the eye. Long dashed line: regression of Aarhus data for $x=0$, 0.08, and 0.10 to Eq. (44), used here to predict D for $x=0.09$, $T=850$ °C. Solid line: slope predicted for D^{int} at 850 °C from Eq. (39) assuming $\tilde{A}=0$ and $\tilde{V}$ for alloys is the same as that measured for $x=0$ in this work; vertical offset is arbitrary.

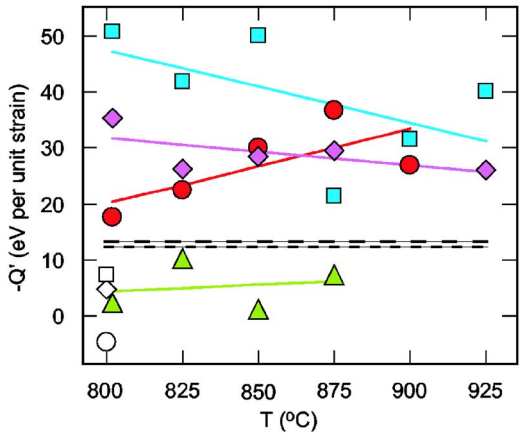

FIG. 6. (IRRATA CORRECTED) Biaxial strain coefficient vs T for various compositions determined by our analysis of the data of Zangenberg *et al.* (FILLED symbols) and Kuo *et al.* (OPEN symbols) for boron diffusion in Si and Si-Ge alloys. Zangenberg data: FILLED squares: 24% Ge, compressive; FILLED diamonds: 12% Ge, compressive; FILLED circles: 0% Ge, tensile; FILLED triangles: 12% Ge, tensile. Kuo data: OPEN square: 20% Ge, compressive; OPEN diamond: 11% Ge (tensile and compressive); OPEN circle: 0% Ge, tensile. Sloping lines are linear fits to the data. Dashed lines are prediction of Eq. (39) with $\tilde{A}=0$ (Table II, sixth column) using our measured $\tilde{V}$ values at 850 °C in Si (long dashed line) and $Si_{89}Ge_{11}$ (short dashed line); dashed lines are drawn horizontal because there is insufficient information to predict a slope.

anisotropies under various sets of assumptions are presented in Table IV.

C. Comparison to B diffusion under biaxial strain

The separate effects of strain and of Ge composition on B diffusion were first measured by Kuo *et al.*[4] at 800 °C and, more recently, over a wide range of temperatures by Zangenberg *et al.*,[38] who also made sufficiently thorough measurements to evaluate the temperature dependence of the strain dependence of D. Zangenberg *et al.* identified Q' in their study as the strain derivative of the apparent activation enthalpy rather than as the strain derivative of the apparent Gibbs free energy of activation, in contrast to previous work[33,34] defining this parameter according to Eq. (37). Additionally, their method for evaluating Q' effectively takes two numerical derivatives of their data, which may introduce unnecessary noise into the result. We retained the original definition of Q', Eq. (37), and extracted values of Q' and other parameters characterizing the diffusion from their results using the linear regression implied by Eq. (44). We reevaluated the biaxial strain in both the Kuo and Zangenberg studies from the reported alloy compositions and the mechanical properties determined in Appendixes B and C.

A linear regression of $\ln D$ against $-1/kT$, $-\varepsilon_{\text{biax}}/kT$, and $-x/kT$, performed according to Eq. (44) for the 43 unique data points of Zangenberg *et al.* with $x=0$, 0.01, 0.12, and 0.24, yields $D_0=10^{(-0.69\pm0.43)}$ cm^2/s, corresponding to $\tilde{S}_{33}/k=5.4\pm1.0$ at 857 °C (assuming $\nu=10^{13}$ Hz), $Q'=(-23.9\pm2.1)$ eV per unit strain, an apparent activation enthalpy of $\tilde{H}_{33}=(3.3\pm0.1)$ eV, and a composition derivative of the apparent free energy of activation of $Q'_x=(0.15\pm0.04)$ eV per unit composition. However, systematic deviations in the data from the regression results cause us to question the validity in the Si-Ge-B system of the Taylor expansion of $\tilde{G}_{33}$ [Eq. (44)]. We conjecture that an unusually large splitting of the degeneracy of energy levels important in the point defect formation or migration process is rendering the Taylor expansion invalid. Consequently we examine subsets of the data to analyze the trends.

Strained and relaxed pairs of samples were annealed under identical conditions for the compositions $x=0$, 0.12, and 0.24, and so for each pair at each temperature a value of Q' may be determined by using Eq. (37). These results, plotted in Fig. 6, show marked variations in Q' with composition and, in some cases, with temperature. Q' for the tensile-relaxed $x=0.12$ alloy pairs (triangles) is much smaller in magnitude than for the compressive-relaxed alloy pairs of the same composition (diamonds). The $-Q'$ values of the tensile-relaxed unalloyed Si pairs (filled circles) display a significant slope of (0.13 ± 0.08) eV/K. The Q' values of the alloys are statistically insignificant or barely significant.[72] In Table V we report the results of a linear regression of $\ln D$ against $-1/kT$ and $-\varepsilon_{\text{biax}}/kT$ spanning all temperatures for

TABLE V. Boron diffusion under biaxial strain. Experimental and theoretical biaxial strain effects on diffusion in Si and $Si_{1-x}Ge_x$; implications using Eq. (39) assuming interstitialcy mechanism. CVD results from Kuo *et al.*; MBE results from Zangenberg *et al.* Among the right-most three columns, bold values are determined directly from experiment (CVD, MBE) or atomistic calculation (GGA); other values result from our interpretation.

Measurement/Calculation, biaxial stress	No. of D data points	x	T (°C)	Q' (eV)	$\tilde{V}/\Omega$ if $\tilde{A}=0$	$\tilde{A}$ if $\tilde{V}$ is as measured
CVD Si (tensile)	3	0	800	+4.6±2.4	−1.34±0.17	1.18±0.22
MBE Si (tensile)	10	0	800–900	−26.6±2.9	0.93±0.21	−1.08±0.26
CVD tensile+compressive $Si_{89}Ge_{11}$	3	0.11	800	−4.9±1.5	−0.65±0.11	0.62±0.13
MBE tensile+compressive $Si_{88}Ge_{12}$	15	0.12	800–925	−18.1±2.2	0.34±0.16	−0.37±0.19
CVD tensile $Si_{89}Ge_{11}$	2	0.11	800	−2.3	−0.83	0.80
MBE tensile $Si_{88}Ge_{12}$	8	0.12	800–875	−6.0±1.9	−0.56±0.14	0.53±0.17
CVD compressive $Si_{89}Ge_{11}$	2	0.11	800	−7.4	−0.46	0.43
MBE compressive $Si_{88}Ge_{12}$	10	0.12	800–925	−28.6±2.0	1.12±0.14	−1.15±0.17
CVD $Si_{80}Ge_{20}$	4	0.2	800	−5.8±2.1	−0.57±0.16	0.54±0.19[a]
MBE compressive $Si_{76}Ge_{24}$	12	0.24	800–925	−39.8±3.9	1.99±0.28	−2.02±0.31
All CVD alloys	7	0.1-0.2	800	−5.7±1.0	−0.58±0.07	0.55±0.10[a]
All MBE alloys	27	0.21–0.24	800–925	−23.4±2.7	0.74±0.20	−0.77±0.23[a]
GGA Si Windl ($\tilde{A}=0$)		0	−273	−10.2	$V^*/\Omega=-0.26$	
GGA Si Windl (extreme $\tilde{A}$)		0	−273	+0.8		≤0.8

[a]Because we have not measured $\tilde{V}$ for the ~20% Ge alloys, we have assumed that its value is the same as we measure for the ~10% Ge alloys.

the five tensile-relaxed unalloyed Si pairs, the four tensile-relaxed $x=0.12$ alloy pairs, the five compressive-relaxed $x=0.12$ alloy pairs, the combined tensile-relaxed-compressive $x=0.12$ alloy samples, and the six compressive-relaxed $x=0.24$ alloy pairs. Q' for tensile Si and for all compressive alloys is large and negative, whereas it is small and negative for the tensile $x=0.12$ alloys. The results of a similar treatment of the data of Kuo *et al.* are also reported in Table V. For all compositions, Kuo's results are characterized by a value of Q' much less negative than are Zangenberg's results, with an extreme case of Kuo's unalloyed Si displaying the only positive value of Q'. The Q' values reported for Zangenberg in Table V are for the average anneal temperature; however, when the best-fit value of Q' at 800 °C is compared directly with Kuo's results at that temperature in Fig. 6, the discrepancy is still apparent.[73] Despite the discrepancies, in both studies tensile ~10% Ge alloys are characterized by a value of Q' substantially less negative than compressive alloys of the same composition. For this reason we report separately for these alloys the results of combining tensile and strain-free alloys of the same composition and combining compressive and strain-free alloys of the same composition.

There is evidence that boron diffusion in dilute $Si_{1-x}Ge_x$ alloys may be significantly different than in unalloyed Si. Kuo *et al.* suggested that B-Ge pairing might be important, and evidence for clustering has been observed recently.[74] Zangenberg *et al.* found that as little as 1% Ge causes a significant (~0.4 eV) increase in the apparent activation energy for B diffusion in Si. Although the interstitialcy mechanism still appears to predominate boron diffusion in dilute Ge alloys,[28] it is possible that diffusion in the alloys is dominated by a different ground-state–saddle-point combination than in Si. It is also possible that strain breaks a ground-state or saddle-point degeneracy in such a way that different ground-state–saddle-point combinations predominate in tensile and compressive materials of the same composition. Although the Gibbs free energy of activation is necessarily close for competing mechanisms $\tilde{H}$, V^*, and Q' may differ markedly.

We now consider the biaxial and hydrostatic stress effects on diffusion together. In Fig. 7 we show the biaxial strain dependence of the 800 °C diffusivities measured by Kuo and Zangenberg. In panels a, b, and c we show the results for unalloyed Si, ~10% Ge alloys, and ~20% Ge alloys, respectively.[75] As these 800 °C plots include only a small subset of the Zangenberg data, we also include, as thin solid lines, the prediction for 800 °C of the regression results from the appropriate Zangenberg samples at all T. More weight should be assigned to the data of Zangenberg *et al.* than to those of Kuo *et al.* due to Zangenberg's large number of data points at nearby temperatures.

The values of Q' predicted from Eq. (39) using the measured values of $\tilde{V}$ and assuming $\tilde{A}=0$ are shown in Table II, and the corresponding slopes are indicated as thick solid lines in Fig. 7. These should be compared against the data points themselves and against the slopes of the thin solid lines. The only case in which any single data set appears to match the predicted slope is for the Zangenberg MBE $Si_{88}Ge_{12}$ when the tensile, strain-free, and compressive samples are considered together (panel b of Fig. 7). This alloy composition, however, is the only one for which we can evaluate the effects of biaxial tension and compression separately, and the evidence is that the behavior is character-

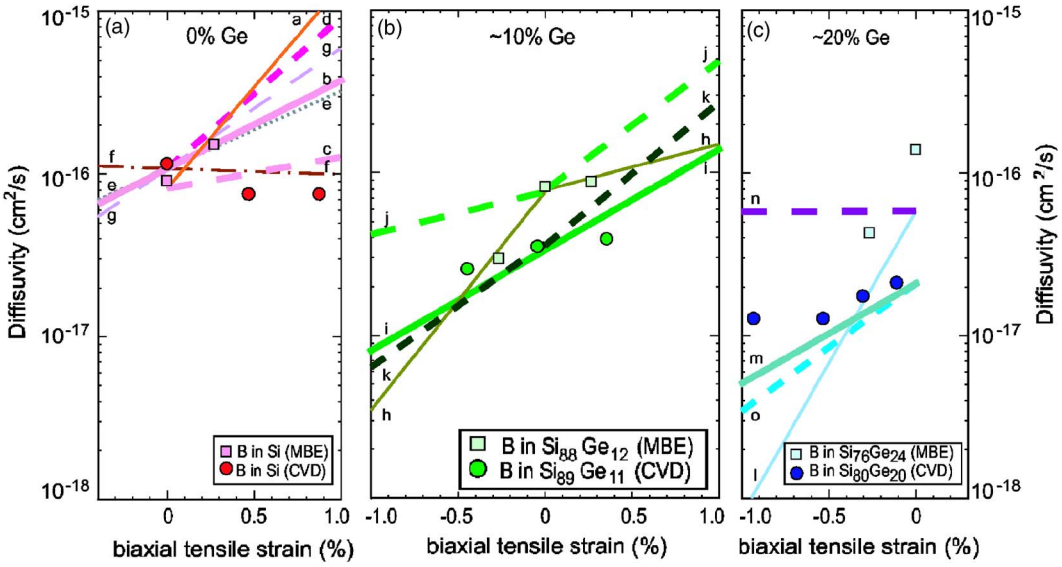

FIG. 7. (Color online) Biaxial strain effect on vertical (D_{33}) and lateral (D_{11}) boron diffusion in Si [panel (a)] and Si-Ge alloys [panel (b), ~10% Ge; panel (c), ~20% Ge]. Circles are Kuo *et al.*'s measurements of D_{33}^{int} in their CVD-grown samples at 800 °C. In all panels, squares are 800 °C subset of the data of Zangenberg *et al.* data for extrinsic D_{33} at 800 °C in their MBE-grown samples; thin solid lines labeled (a), (h), and (l) are predictions for 800 °C of regression to all Zangenberg data spanning range 800–925 °C. Thick solid lines labeled (b), (i), and (m) are vertical diffusivities D_{33} predicted by Eq. (39) assuming $\tilde{A}=0$ and using our measured values of $\tilde{V}$ for unalloyed Si in (b) and for CVD $Si_{89}Ge_{11}$ in (i); (m) assumes $\tilde{V}$ for $Si_{80}Ge_{20}$ is same as that measured for $Si_{89}Ge_{11}$. Dashed lines indicate lateral diffusivities D_{11} predicted by Eq. (47) using anisotropy from final column of Table V. Short dashed lines labeled (d), (k), and (o) are predictions using results from Kuo's CVD-grown samples; long dashed lines labeled (c), (j), and (n) are predictions using results from Zangenberg's MBE-grown samples. In panel B, tensile alloys and compressive alloys are treated as different materials and separate regressions have been performed for (tensile+strain-free) and for (compressive+strain-free), resulting in slope discontinuities at zero strain. The *ab initio* (GGA) calculations of Windl and coworkers' for hexagonal boron interstitial saddle point in unalloyed Si assuming $\tilde{A}=0$ are thin broken lines in panel (A). Thin dot-dashed (f) and dotted (e) lines are D_{33} with $\tilde{A}$ equal to extreme value (0.8) and zero, respectively, as discussed in text; in the latter case the line also represents the predicted behavior of D_{11}. Also indicated by thin dashed line (g) is prediction for D_{11} from GGA calculations with extreme value of $\tilde{A}$.

ized by a different slope on each side of zero strain: the thin solid lines in panel b, representing regressions to the Zangenberg tensile and compressive data, have very different slopes from each other. And the slope of neither matches the slope predicted by Eq. (39).

The anisotropy required to exactly reconcile the hydrostatic and each set of biaxial results is shown in Table V. In contrast to the Sb diffusion results (for which the inferred value of $\tilde{A}$ for all but the Portavoce $x=0.09$ alloys was rather close to zero), the inferred value of $\tilde{A}$ for all boron samples is relatively large in magnitude. Although in all cases except the tensile ~10% Ge alloys the results inferred from Kuo's CVD and Zangenberg's MBE samples bracket $\tilde{A}=0$, in no case is the required anisotropy zero within the stated error bar. It is not obvious that we can ascribe the disagreement between the Kuo (CVD) and Zangenberg (MBE) results to the difference in growth technique, as we measure the same value of $\tilde{V}$ in MBE and CVD unalloyed Si. We conclude that the hydrostatic and biaxial data are not consistent with Eq. (39) with $\tilde{A}=0$, no matter which biaxial data sets are considered.

This disagreement between experimental Q' values and values predicted from Eq. (39) using hydrostatic compression experiments and assuming $\tilde{A}=0$ stands in marked contrast to the agreement, discussed earlier, for Sb. Agreement is also obtained in the case of phosphorus, another consensus interstitial-based diffuser such as boron.[76]

Is it plausible that $\tilde{A}$ differs significantly from zero for boron diffusion in Si and dilute Ge alloys? On the one hand, based on crystallography $A=0$ is expected in the theory of Daw *et al.*[14] from an interstitialcy mechanism with a hexagonal saddle point and the BI^+ ground state. It is not obvious why biaxial strain of an (001) film should affect D_{33} the same as it affects D_{11} within the context of the theory, but we advance the following conjecture. Although the direction of point defect motion is not along a ⟨111⟩, in transition state theory a particular BI^+ "potential well" is in equilibrium with all symmetry-equivalent saddle points and the energy landscape in between well and saddle point doesn't matter. The long-range dilatation at each BI^+ potential well and at each saddle point can be represented by an ellipsoid of revolution with a ⟨111⟩ symmetry axis. Biaxial compression can be represented as a superposition of hydrostatic compression and uniaxial tension along [001]. The energies of all the potential wells must be affected the same way by hydrostatic compression. The energies of all the saddle points must be affected the same way by hydrostatic compression. The energies of all the potential wells must be affected the same way by uniaxial tension along [001]. And the energies of all the

saddle points must be affected the same way by uniaxial tension along [001]. So the barrier to net motion along [001] and the barrier to net motion along, say, [100] has the same height for any biaxial strain state—i.e., Γ remains isotropic even under biaxial strain.

On the other hand, it is not clear how much anisotropy can be introduced by a saddle point that is near, but not precisely at, a hexagonal interstitial position. It is also possible that the approximations inherent in LDA and GGA, or the determination of energies at absolute zero, are insufficient to correctly identify the actual dominant transport path in physical experiments at ~1100 K. Furthermore it is not impossible that, even if $A=0$, $|\tilde{A}|\sim 1$ due to the stress dependence of the correlation factor. This possibility has not been addressed theoretically. Nevertheless, the wide scatter in the inferred values of $\tilde{A}$ in Table V indicate that something is amiss. Could the anisotropy in the correlation factor vary widely with Ge composition, with the transition from biaxial tension to biaxial compression, or with trace impurity content that may vary from laboratory to laboratory?

The *ab initio* calculations of Windl and co-workers[30,31] permit the anisotropic strains in the point defect ground state and saddle point to be identified and Q' to be predicted theoretically. For a Fermi level slightly below midgap, the formation strain tensor for BI^+ from a buried B^+ and a silicon atom at a kink site on a surface step is predicted,[77] from GGA, to be

$$\mathbf{V}^f = -\Omega\begin{bmatrix} 0 & 0 & 0 \\ 0 & 0 & 0 \\ 0 & 0 & 1 \end{bmatrix} + \Omega\begin{bmatrix} 0.23 & 0 & 0 \\ 0 & 0.23 & 0 \\ 0 & 0 & 0.095 \end{bmatrix}. \quad (45)$$

The above representation is for a (111) wafer with the third Cartesian coordinate in the [111] direction and the first two Cartesian coordinates orthogonal to it and to each other. This representation is chosen for convenience because in it the formation strain tensor is diagonal. It can be seen that the distortion of the crystal is oblate with a [111] symmetry axis. At each lattice point there are four energetically degenerate orientations for the BI^+, with the B-I bond pointing in the opposite direction to each of the ⟨111⟩ bonds between boron and a substitutional silicon. The (nearly) saddle point calculation for the neutral ring-center (H^0) yields a distortion with a ⟨111⟩ symmetry axis that is, curiously, prolate. However, the only direct pathways that have been found are between ground states and ring centers with nonparallel ⟨111⟩ axes.[77] The magnitude of the migration strain anisotropy for such pathways has an upper limit of the anisotropy between a transition from the oblate $[111]BI^+$ to the parallel, but prolate, $[111]H^0$. The migration strain tensor for this latter transition, between configurations with parallel symmetry axes, is

$$\mathbf{V}^m_{\text{extreme}} = \Omega\begin{bmatrix} -0.21 & 0 & 0 \\ 0 & -0.21 & 0 \\ 0 & 0 & +0.59 \end{bmatrix}, \quad (46)$$

from which an upperlimiting anisotropy of $A=+0.8$ may be identified. The corresponding lowerlimiting value of the magnitude of the anisotropy is $A=0$, which results from the combinatorics.[14] associated with stress effects on the paths that contribute to D_{33} between multiply degenerate defects with the symmetries described above, assuming the hexagonal site to be the true saddle point.[78] We can provisionally view these values of A as the extreme values of anticipated behavior of $\tilde{A}$ (Ref. 79) and examine their implications for diffusion under biaxial strain. Inserting these extreme values of 0 and +0.8 for $\tilde{A}$ into Eq. (38) we obtain values of Q' of −10.2 eV and +0.8 eV, respectively; these are identified as GGA in Table V. Note that the inferred values of Q' for *both* MBE and CVD tensile Si near the top of the same column in Table V, as well as the inferred values of $\tilde{A}$ in the seventh column, lie outside these "bounds," but in opposite directions. In panel (A) of Fig. 7 we show the GGA prediction for D_{33} and D_{11} (curves f and g, respectively) with $\tilde{A}=+0.8$, and the GGA prediction for the resulting isotropic diffusivity with $\tilde{A}=0$ (curve e).

From these comparisons, we view the large value of $\tilde{A}=+1.18$ for CVD Si and −1.08 for MBE Si obtained by the combination of hydrostatic and biaxial measurements with skepticism. The possibility of experimental artifacts and theoretical over-simplifications are strong motivation for further research. A measurement of a strain effect independent of the hydrostatic and biaxial strain effects on D_{33} would provide very valuable complementary information. One such experiment would be the effect of in-plane biaxial stress upon D_{11}, the diffusivity in a direction parallel to the surface. From Eq. (32) and the analogous equation for D_{11}, the anisotropy in the migration volume can be determined directly from such an experiment:

$$\frac{D_{11}(\sigma_{\text{biax}})}{D_{33}(\sigma_{\text{biax}})} = \exp\left[\left(\frac{\sigma_{\text{biax}}\Omega}{kT}\right)\tilde{A}\right]. \quad (47)$$

Our predictions for D_{11} from Eq. (47), using values of the migration strain anisotropy inferred from the measurements of Q' and $\tilde{V}$ in Table V, are shown as dashed lines in Fig. 7.

VI. SUMMARY AND CONCLUSIONS

(1) The intrinsic diffusivity of MBE-grown Sb doping superlattice spikes in Si is retarded slightly by hydrostatic pressure, characterized by an apparent activation volume of $\tilde{V}=(+0.06\pm0.04)\ \Omega$.

(2) The measured $\tilde{V}$ for Sb diffusion in Si is close to the values predicted for the vacancy mechanism by various *ab initio* calculations assuming a pressure-independent correlation factor, but the theoretical result is unsettled.

(3) The intrinsic diffusivity of MBE-grown boron doping superlattice spikes in Si is enhanced by hydrostatic pressure, characterized by $\tilde{V}=(-0.16\pm0.05)\ \Omega$.

(4) The intrinsic diffusivity of boron in CVD-grown Si films is enhanced by hydrostatic pressure, characterized by $\tilde{V}=(-0.16\pm0.05)\ \Omega$.

(5) The intrinsic diffusivity of boron in strain-relaxed CVD-grown $Si_{89}Ge_{11}$ films is imperceptibly pressure dependent, characterized by $\tilde{V}=(-0.03\pm0.03)\ \Omega$.

(6) The measured $\tilde{V}$ for boron diffusion in Si is close to the value predicted for the interstitialcy mechanism by *ab initio* calculations assuming a pressure-independent correlation factor.

(7) A thermodynamic treatment of diffusion under hydrostatic and nonhydrostatic stress is developed for sample configurations in which virtually all point defect equilibration occurs at the free surface of a hydrostatically or biaxially strained thin film stack. Relationships are predicted between the effects of hydrostatic and biaxial stress on diffusion normal to the surface, Eq. (39), and parallel to the surface, Eq. (47).

(8) Literature data for Sb and B diffusion in relaxed and strained Si and dilute Si-Ge alloys are reanalyzed to provide a consistent method of extracting materials parameters such as Q'.

(9) For Sb diffusion, the experimental results are consistent with the predicted relationship, (39), between vertical diffusion under hydrostatic and biaxial stress, assuming a vacancy mechanism with near zero apparent migration strain anisotropy. This result confirms the value of the approach, lends further support to the consensus that Sb diffuses by virtually a pure vacancy mechanism, and demonstrates progress toward predictive capability for the effect of nonhydrostatic stress on diffusion.

(10) For B diffusion, none of the experimental results for Q' is consistent with the hydrostatic measurements of $\tilde{V}$ and the predicted relationship, (39) assuming an interstitial-based mechanism with zero or small apparent migration strain anisotropy. This discrepancy does not appear to reflect a fundamental limitation of the theoretical approach for interstitial-based mechanisms, as the approach is known to work well for phosphorus, another virtually 100% interstitial diffuser in Si. Furthermore, the experimental data series for Q' are widely inconsistent among themselves.

(11) A measurement of the effect of biaxial strain on diffusion in a direction parallel to the surface, used with Eq. (47), could help resolve these discrepancies.

ACKNOWLEDGMENTS

We are grateful to J.L. Hoyt for providing Kuo's CVD Si(B) and SiGe(B) samples, to W. Windl for communicating unpublished results of *ab initio* calculations of the volumetrics of boron diffusion in Si, to W. Windl, M.S. Daw, B. Sadigh, R.C. Cammarata, and F. Spaepen for helpful discussions on theoretical issues, to J.L. Hoyt, I. Berbezier, and A. Nylandsted Larsen for helpful discussions about their experiments, and to J.F. Sage and F. Spaepen for a critical reading of the manuscript. Work at Harvard was supported by NSF Grant No. DMR-0213373 and at LANL was supported by the Division of Materials Sciences, DOE under Contract No. W-7405-ENG-36 with the University of California.

APPENDIX A: RELATION BETWEEN FORMATION VOLUME AND PRESSURE-DEPENDENT FORMATION ENERGY

The Gibbs free energy of point defect formation G^f for a doped semiconductor under hydrostatic pressure may be written

$$G^f(T,P,x,C) = F^f(T,P,x,C) + PV^f(T,P,x,C), \quad \text{(A1)}$$

where x is the alloy composition, C is the dopant concentration, and the Helmholtz free energy of formation F^f involves electronic contributions from the charge state of the defect, the Fermi level, band-bending effects, and shifts in defect and ground-state energy levels due to strain. Baumann *et al.*[9] advance a specific form for $F^f(T,P,x,\mu_F,\varepsilon_{\text{biax}})$, where the Fermi level μ_F is chosen instead of C as an independent variable. Their treatment is nominally for biaxial strain but actually more appropriate for hydrostatic pressure; furthermore P and $\varepsilon_{\text{biax}}$ are not independent in samples with a free surface. The pressure derivative of Eq. (A1) is

$$\left.\frac{\partial G^f}{\partial P}\right|_{T,x,C} = \left.\frac{\partial F^f}{\partial P}\right|_{T,x,C} + P\left.\frac{\partial V^f}{\partial P}\right|_{T,x,C} + V^f. \quad \text{(A2)}$$

But $dF=-S\,dT+P\,dV$ for systems with constant numbers of species, implying

$$\left.\frac{\partial F^f}{\partial P}\right|_{T,x,C} = -P\left.\frac{\partial V^f}{\partial P}\right|_{T,x,C}, \quad \text{(A3)}$$

resulting in

$$\left.\frac{\partial G^f}{\partial P}\right|_{T,P,x,C} = V^f(T,P,x,C). \quad \text{(A4)}$$

From this result we conclude that any interpretation accounting for the first term but not the second term on the right-hand side (RHS) of Eq. (A2) is flawed. This result does not imply that electronic contributions are negligible; it means only that they are accounted for in V^f. For example, the formation volume of a negative vacancy differs, perhaps quite substantially, from that of a neutral vacancy, by the volume change of the crystal upon moving an electron, at constant P, from the Fermi level to a localized state on the vacancy. This conclusion generalizes straightforwardly to nonhydrostatic stress states for the case treated in this paper of point defect equilibration at the top surface of a film stack.

APPENDIX B: ESTIMATION OF BIAXIAL MODULUS AT HIGH TEMPERATURE

The biaxial modulus is defined as

$$Y = E/(1-\nu), \quad \text{(B1)}$$

where E is the Young's modulus and ν is the Possion's ratio. E and ν are determined by the components of the elastic stiffness tensor or elastic compliance tensor for the solid.

For Si, temperature-dependent values for the component of the elastic stiffness tensor s_{11}, and for two components of the elastic compliance tensor c_{11} and c_{12} are known.[80] For biaxial stress in the Si(001) plane, E and ν are expressed, respectively, as

$$E = 1/S_{11}, \quad \text{(B2)}$$

$$\nu = c_{12}/(c_{11}+c_{12}). \quad \text{(B3)}$$

For Ge the measured values are known[81] for c_{11} and cs, which is defined as $cs=(c_{11}-c_{12})/2$. For biaxial stress in the

TABLE VI. Fitting parameters obtained from the best fit of empirical data to Eq. (B6).

	Elastic constants	a	b	c
Si	$s_{11}(10^{-13}\ \mathrm{cm^2/dyn})$	3.1020×10^{-7}	2.6613×10^{-4}	7.6626
	$c_{11}(10^{11}\ \mathrm{dyn/cm^2})$	-6.4311×10^{-7}	-5.1208×10^{-4}	16.2250
	$c_{12}(10^{11}\ \mathrm{dyn/cm^2})$	-4.1687×10^{-7}	1.7696×10^{-5}	5.8248
Ge	$c_{11}(10^{11}\ \mathrm{dyn/cm^2})$	-4.8758×10^{-7}	-1.1612×10^{-3}	12.8390
	$cs(10^{11}\ \mathrm{dyn/cm^2})$	-3.5593×10^{-8}	-5.1577×10^{-4}	4.2583

Ge(001) plane, E and ν are expressed, respectively, as

$$E = (c_{11}+2c_{12})(c_{11}-c_{12})/(c_{11}+c_{12}) = cs(3c_{11}-4cs)/(c_{11}-cs) \tag{B4}$$

$$\nu = c_{12}/(c_{11}+c_{12}) = (c_{11}+2cs)/2(c_{11}-cs) \tag{B5}$$

We fit s_{11}, c_{11}, and c_{12} for Si, and c_{11} and cs for Ge, respectively, to a quadratic function $y(T)$ of absolute temperature

$$y = aT^2 + bT + c. \tag{B6}$$

We observe that Eq. (B6) fits all the empirical data very well. Table VI lists the values of the fitting parameters for the best fits. Using Eqs. (B1)–(B6) we calculate the biaxial modulus $Y_{\mathrm{Si}}(T)$ for Si and $Y_{\mathrm{Ge}}(T)$ for Ge at a given temperature T.

The biaxial modulus $Y(T,x)$ for a $\mathrm{Si}_{1-x}\mathrm{Ge}_x$ alloy at T is estimated by linear composition-weighted interpolation between $Y_{\mathrm{Si}}(T)$ and $Y_{\mathrm{Ge}}(T)$:

$$Y(T,x) = (1-x)Y_{\mathrm{Si}}(T) + xY_{\mathrm{Ge}}(T). \tag{B7}$$

APPENDIX C: ESTIMATION OF ATOMIC VOLUME AT HIGH TEMPERATURE

The lattice parameter $a_0(T)$ for Si and Ge at temperature T is calculated using the expression

$$a_0(T) = a_0(273)\cdot\left\{1+\int_{273}^{T}\alpha(T')dT'\right\}, \tag{C1}$$

where $\alpha(T)$ is the liner thermal expansion coefficient for Si or Ge. It has been shown[82] that the temperature dependence of $\alpha(T)$ for Si is empirically fit well by

$$\alpha(T) = (3.725\{1-\exp[-5.88\times10^{-3}(T-124)]\} + 5.548\times10^{-4}T)\times10^{-6}(\mathrm{K}^{-1}), \tag{C2}$$

with T in K, over the temperature range 120 to 1500 K. We fit measured data[83] for $a_0(T)$ for Ge from 120 to 1200 K using the same form as Eq. (C2) and obtain

$$\alpha(T) = (5.231\{1-\exp[-9.60\times10^{-3}(T-14.9)]\} + 3.300\times10^{-3}T)\times10^{-6}(\mathrm{K}^{-1}). \tag{C3}$$

Substituting Eq. (C2) or Eq. (C2) into Eq. (C1) with $a_0(273.2)=0.5430741$ nm for Si and $a_0(273.2)=0.565750$ nm for Ge, we calculate the temperature-dependent lattice parameters for Si and Ge. We evaluate the temperature-dependent atomic volume $\Omega_{\mathrm{Si}}(T)$ and $\Omega_{\mathrm{Ge}}(T)$ as one-eighth of the cube of the appropriate lattice parameter.

The atomic volume $\Omega(T,x)$ for a $\mathrm{Si}_{1-x}\mathrm{Ge}_x$ alloy at temperature T is calculated by linear composition-weighted interpolation between $\Omega_{\mathrm{Si}}(T)$ and $\Omega_{\mathrm{Ge}}(T)$:

$$\Omega(T,x) = (1-x)\Omega_{\mathrm{Si}}(T) + x\Omega_{\mathrm{Ge}}(T). \tag{C4c}$$

*Electronic address: maziz@harvard.edu

†Present address: NovaStrata, 3432 Denmark Ave. No. 166, Eagan, MN 55123.

[1] H. Park, K. S. Jones, J. A. Slinkman, and M. E. Law, J. Appl. Phys. **78**, 3664 (1995).

[2] M. J. Aziz, Appl. Phys. Lett. **70**, 2810 (1997).

[3] M. J. Aziz, in *Defects and Diffusion in Silicon Processing*, edited by T. Diaz de la Rubia *et al.*, MRS Symp. Proc. No. 469 (Materials Research Society, Pittsburgh, 1997), p. 37.

[4] P. Kuo, J. L. Hoyt, J. F. Gibbons, J. E. Turner, and D. Lefforge, Appl. Phys. Lett. **66**, 580 (1995).

[5] P. M. Fahey, P. B. Griffin, and J. D. Plummer, Rev. Mod. Phys. **61**, 289 (1989).

[6] H.-J. Gossmann, T. E. Haynes, P. A. Stolk, D. C. Jacobson, G. H. Gilmer, J. M. Poate, H. S. Luftman, T. K. Mogi, and M. O. Thompson, Appl. Phys. Lett. **71**, 3862 (1997).

[7] K. C. Pandey and E. Kaxiras, Phys. Rev. Lett. **66**, 915 (1991).

[8] H^f is a thermodynamic potential given the same assumptions permitting G^f to be a thermodynamic potential.

[9] F. H. Baumann, J.-H. Huang, J. A. Rentschler, T. Y. Chang, and A. Ourmazd, Phys. Rev. Lett. **73**, 448 (1994).

[10] In the context of Eq. (8), the last term in Eq. (9) is the change in work done by external tractions on the film due to a stress-induced change in formation volume.

[11] M. J. Aziz, P. C. Sabin, and G.-Q. Lu, Phys. Rev. B **44**, 9812 (1991).

[12] G. H. Vineyard, J. Phys. Chem. Solids **3**, 121 (1957).

[13] L. D. Landau and E. M. Lifshitz, *Statistical Physics* (Pergamon, New York, 1969).

[14] M. S. Daw, W. Windl, N. N. Carlson, M. Laudon, and M. P. Masquelier, Phys. Rev. B **64**, 045205 (2001).

[15] J. R. Rice, J. Mech. Phys. Solids **19**, 433 (1971); J. R. Rice, in *Constitutive Equations in Plasticity*, edited by A. S. Argon (MIT Press, Cambridge, 1975), pp. 23–79.

[16] J. R. Manning, Phys. Rev. Lett. **1**, 365 (1958); J. G. Mullen, Phys. Rev. **124**, 1723 (1961); A. D. LeClaire, Philos. Mag. **7**, 141 (1962); J. R. Manning, Phys. Rev. **136**, A1758 (1964).

[17] S. M. Hu, Phys. Status Solidi B **60**, 595 (1973).

[18] S. T. Dunham and C. D. Wu, J. Appl. Phys. **78**, 2362 (1995); O. Pankratov, H. C. Huang, T. D. delaRubia, and C. Mailhiot, Phys. Rev. B **56**, 13172 (1997).

[19] P. Ramanarayanan, B. Srinivasan, K. Cho, and B. M. Clemens, J. Appl. Phys. **96**, 7095 (2004).

[20] We also permit ν to depend smoothly on ambient conditions, although we expect this dependence always to be very weak. We assume g to be truly constant and neglect the variation of a with the understanding that composition profiling before and after diffusion anneals are performed at the same T, P, and x, thereby negating the effect of any dependence of a on these variables.

[21] This is reasonable given the established relationships between free energies, jump frequencies, and correlation factors as described, e.g., by Vineyard in Ref. 12 and Manning in Ref. 16. Note also that the pre-exponential factors f and ν can differ for D_{33} and D_{11} after a tetragonal distortion caused by biaxial strain as discussed in part Mullen in Ref. 16.

[22] N. L. Peterson, Solid State Phys. **22**, 409 (1968).

[23] A. Antonelli and J. Bernholc, Phys. Rev. B **40**, 10643 (1989); A. Antonelli and J. Bernholc, in *Impurities, Defects and Diffusion in Semiconductors: Bulk and Layered Structures*, edited by D. J. Wolford, J. Bernholc, and E. E. Haller, MRS Symp. Proc. No. 163 (Materials Research Society, Pittsburgh, 1990), p. 523; M. Tang, L. Colombo, J. Zhu, and T. Diaz de la Rubia, Phys. Rev. B **55**, 14279 (1997).

[24] A. Antonelli, E. Kaxiras, and D. J. Chadi, Phys. Rev. Lett. **81**, 2088 (1998).

[25] O. Sugino and A. Oshiyama, Phys. Rev. B **46**, 12335 (1992).

[26] S. Matsumoto, Y. Ishikawa, and T. Niimi, J. Appl. Phys. **54**, 5049 (1983); D. Mathiot and J. C. Pfister, *ibid.* **55**, 3518 (1984).

[27] A. Ural, P. B. Griffin, and J. Plummer, J. Appl. Phys. **85**, 6440 (1999).

[28] T. T. Fang, W. T. C. Fang, P. B. Griffin, and J. D. Plummer, Appl. Phys. Lett. **68**, 791 (1996).

[29] B. Sadigh, T. J. Lenosky, S. K. Theiss, M.-J. Caturla, T. Diaz de la Rubia, and M. A. Foad, Phys. Rev. Lett. **83**, 4341 (1999).

[30] W. Windl, M. M. Bunea, R. Stumpf, S. T. Dunham, and M. P. Masquelier, Phys. Rev. Lett. **83**, 4345 (1999).

[31] M. Laudon, N. N. Carlson, M. P. Masquelier, M. S. Daw, and W. Windl, Appl. Phys. Lett. **78**, 201 (2001).

[32] N. Moriya, L. C. Feldman, H. S. Luftman, C. A. King, J. Bevk, and B. Freer, Phys. Rev. Lett. **71**, 883 (1993); P. Kuo, J. L. Hoyt, J. F. Gibbons, J. E. Turner, R. D. Jacowitz, and T. I. Kamins, Appl. Phys. Lett. **62**, 612 (1993); K. Rajendran and W. Schoenmaker, J. Appl. Phys. **89**, 980 (2001); J. S. Christensen, H. H. Radamson, A. Y. Kuznetsov, and B. G. Svensson, *ibid.* **94**, 6533 (2003).

[33] N. E. B. Cowern, P. C. Zalm, P. van der Sluis, D. J. Gravesteijn, and W. B. de Boer, Phys. Rev. Lett. **72**, 2585 (1994); N. E. B. Cowern, W. J. Kersten, R. C. M. de Kruif, J. G. M. van Berkum, W. B. de Boer, D. J. Gravesteijn, and C. W. T. Bulle-Liewma, in *Proceedings of the 4th International Symposium on Process Physics and Modeling in Semiconductor Devices*, edited by G. R. Srinivasan, C. S. Murthy, and S. T. Dunham, Electrochemical Society Proceedings No. 96-4 (Electrochemical Society, Pennington, NJ, 1996).

[34] P. Kringhoj, A. N. Larsen, and S. Y. Shirayev, Phys. Rev. Lett. **76**, 3372 (1996).

[35] P. Kringhoj and A. Nylandsted Larsen, Defect Diffus. Forum **143**, 1125 (1997).

[36] A. Y. Kuznetsov, J. Cardenas, D. C. Schmidt, B. G. Svensson, J. L. Hansen, and A. N. Larsen, Phys. Rev. B **59**, 7274 (1999).

[37] A. Portavoce, Ph.D. thesis, Universite de Droit, D'Economie et des Sciences D'Aix-Marseille, 2002.

[38] N. R. Zangenberg, J. Fage-Pedersen, J. L. Hansen, and A. N. Larsen, J. Appl. Phys. **94**, 3883 (2003).

[39] The validity of this equation is not restricted to the case of stress-independent volumes, if Q' is defined as the biaxial strain derivative of $-kT \ln D_{33}$ instead of Eq. (37).

[40] Under point defect equilibrium conditions the effect of stress on ground state energetics cancels out of the expression for the effect of stress on the diffusivity, as shown in P. H. Dederichs and K. Schroeder, Phys. Rev. B **17**, 2524 (1978).

[41] H. J. Gossmann, in *Delta-Doping of Semiconductors*, edited by E. F. Schubert (Cambridge University Press, Cambridge, UK, 1996), p. 161.

[42] H.-J. Gossmann, in *Delta-Doping of Semiconductors*, edited by E. F. Schubert (Cambridge University Press, Cambridge, UK, 1996), p. 253.

[43] W. Kern, *Handbook of Semiconductor Wafer Cleaning Technology: Science, Technology, and Applications* (Noyes, Park Ridge, NJ, 1993).

[44] H.-J. Gossmann, C. S. Rafferty, F. C. Unterwald, and T. Boone, Appl. Phys. Lett. **67**, 1558 (1995).

[45] One ion source (Ion Tech, 2.5 cm) shot 1200 eV Ar^+ at a Si target $\sim$20 cm away; sputtered Si atoms arrived at the growth surface concurrently with 600 eV N_2^+ which was delivered by another, identical ion source aimed directly at the growth surface. The N_2 ions react with Si forming a Si_3N_4 layer that is nearly stoichiometric, as indicated by 2.0 MeV He^+ Rutherford backscattering spectrometry measurements, at a deposition rate of 0.05–0.1 nm/s.

[46] Y. C. Zhao, W. Barvosa-Carter, S. D. Theiss, S. Mitha, M. J. Aziz, and D. Schiferl, J. Appl. Phys. **84**, 4049 (1998).

[47] R. B. Fair, in *Impurity Doping Process in Silicon*, edited by F. F. Y. Wang (North-Holland, Amsterdam, 1981), pp. 315.

[48] H.-J. Gossmann, G. H. Gilmer, C. S. Rafferty, F. C. Unterwald, T. Boone, J. M. Poate, H. S. Luftman, and W. Frank, J. Appl. Phys. **77**, 1948 (1995).

[49] Note that they use the variable D_A for the intrinsic diffusivity and we use it for the extrinsic diffusivity.

[50] This assumption could result in a small error that can be corrected when appropriate data become available. The contributions are known to have the same activation energies for B but different activation energies for Sb. See Ref. 47.

[51] E. R. Johnson and S. M. Christian, Phys. Rev. **95**, 560 (1954).

[52] S. M. Sze, *Physics of Semiconductor Devices* (Wiley, New York, 1981), pp. 245.

[53] W. Paul, J. Appl. Phys. **32**, 2082 (1961).

[54] T. K. Mogi, M. O. Thompson, H.-J. Gossmann, J. M. Poate, and H. S. Luftman, Appl. Phys. Lett. **69**, 1273 (1996).

[55] The run to run reproducibility of D was estimated to be ±12% from the discrepancy between the two samples run at 2.5 GPa, under nominally identical conditions. This leads to an uncertainty in $\tilde{V}$ of ±0.03 Ω. An additional uncertainty of ±0.02 Ω is assumed to account for the possible variation of $\tilde{V}$ with peak number due, e.g., to MBE growth artifacts or surface effects, and is reckoned as the standard deviation of the $\tilde{V}$ values for the six peaks. The squares of these uncertainties were assumed to add.

[56] The diffusivity of interstitials at 860 °C used here is obtained by extrapolation using an estimated activation energy of 3.1 eV of data obtained at 810 °C by Gossmann *et al.* in studies of oxidation enhanced diffusion in boron doping superlattices reported in H. J. Gossmann, G. H. Gilmer, C. S. Rafferty, F. C. Unterwald,

T. Boone, J. M. Poate, H. S. Luftman, and W. Frank, J. Appl. Phys. **77**, 1948 (1995); H. J. Gossmann, C. S. Rafferty, H. S. Luftman, F. C. Unterwald, T. Boone, and J. M. Poate, Appl. Phys. Lett. **63**, 639 (1993).

[57] H. J. Gossmann, C. S. Rafferty, A. M. Vredenberg, H. S. Luftman, F. C. Unterwald, D. J. Eaglesham, D. C. Jacobson, T. Boone, and J. M. Poate, Appl. Phys. Lett. **64**, 312 (1994).

[58] W. T. C. Fang, T. T. Fang, P. B. Griffin, and J. D. Plummer, Appl. Phys. Lett. **68**, 2085 (1996).

[59] An alternative interpretation, that the time scale for self interstitials to reach spikes 2–6 from the surface is much longer than 3 h, and that our measurements therefore yield the migration volume of the B-I complex, seems implausible in light of the measured value of D_I quoted above.

[60] We included a run to run pressure uncertainty of 0.4 GPa; an uncertainty of 7% in D resulting from the uncertainty in temperature reproducibility; and an uncertainty of 7% in D resulting from the uncertainty in concentration depth profiling. An additional uncertainty of $\pm 0.021\ \Omega$ is assumed to account for the possible variation of $\tilde{V}$ with peak number due, e.g., to MBE growth artifacts or surface effects, and is reckoned as the standard deviation of the $\tilde{V}$ values for the six peaks in the 1 h anneal. The squares of all of these uncertainties were assumed to add.

[61] J. Zhu, T. Diaz de la Rubia, L. H. Yang, C. Mailhiot, and G. H. Gilmer, Phys. Rev. B **54**, 4741 (1996).

[62] W. Windl, M. S. Daw, N. N. Carlson, and M. Laudon, in *Advances in Materials Theory and Modeling—Bridging Over Multiple Length and Time Scale*, edited by Vasily Bulotov *et al.*, MRS Symposia Proceedings No. 677 (Materials Research Society, Warrendale, PA, 2001), p. AA9.4.

[63] Y. Zhao, W. Windl, and M. J. Aziz (unpublished).

[64] J. Xie and S. P. Chen, J. Phys. D **32**, 1252 (1999).

[65] P. E. Blochl, C. G. Van de Walle, and S. T. Pantelides, Phys. Rev. Lett. **64**, 1401 (1990).

[66] A. N. Larsen and P. Kringhoj, Phys. Scr. **T69**, 92 (1997); A. Y. Kuznetsov, J. Cardenas, B. G. Svensson, A. N. Larsen, and J. L. Hansen, in *Diffusion Mechanisms in Crystalline Materials*, edited by Y. Mishin, N. E. B. Cowern, C. R. A. Catlow, D. Farkas, and G. Vogl, MRS Symp. Proc. No. 527 (Materials Research Society, Pittsburgh, 1998), p. 435.

[67] The dopant concentration in the samples spans the range from less than to about twice the intrinsic carrier concentration. The authors reported actual diffusivities—not intrinsic diffusivities—and noted that the samples are nearly intrinsic and fit the linear diffusion equation satisfactorily. We have not reanalyzed their results to determine the intrinsic diffusivity.

[68] A. N. Larsen and P. Kringhoj, Appl. Phys. Lett. **68**, 2684 (1996).

[69] By performing the regression as described we are assuming $\tilde{H}_{33}$, Q', and Q'^{x}_{I} are independent of dopant concentration. The maximum anticipated error on Q' from this assumption is estimated to amount to $3\delta Q'/2Y \approx 0.06\ \Omega$ for Kringhoj's peak Sb concentration of $2\times 10/^{19}\ \mathrm{cm}^2$, based on the second factor on the right-hand side of Eq. (42) and the known dependence of band gap on biaxial tension.

[70] A. Portavoce, P. Gas, I. Berbezier, A. Ronda, J. S. Christensen, A. Y. Kuznetsov, and B. G. Svensson, Phys. Rev. B **69**, 155415 (2004).

[71] The authors reported actual diffusivities—not intrinsic diffusivities—but noted that the samples are highly extrinsic. We have not reanalyzed their results to determine the intrinsic diffusivity. By performing the regression as described we are assuming Q', $\tilde{H}_{33}$, and Q'^{x}_{I} are independent of dopant concentration.

[72] Q' of the tensile-relaxed $x=0.12$ alloy pairs, the compressive-relaxed $x=0.12$ alloy pairs, and the compressive-relaxed $x=0.24$ alloy pairs are fit by slopes of $0.02\pm0.09, -0.05\pm0.04$, and -0.13 ± 0.10 eV/K, respectively.

[73] The dopant concentration in the samples in both the Kuo and Zangenberg studies spans the range from much less than to about equal to the intrinsic carrier concentration. Zangenberg reported actual diffusivities whereas Kuo reported intrinsic diffusivities. In making these comparisons we have assumed $\tilde{H}_{33}$, Q', and Q'_x are independent of dopant concentration over this range. The maximum error in Q' due to the strain dependence of the intrinsic carrier concentration is likely to be even smaller than that for Sb noted earlier because the boron concentrations are all smaller than the highest Sb concentrations.

[74] J. Hattendorf, W. Zeitz, W. Schroeder, and N. Abrosimov, Physica B **340**, 858 (2003).

[75] Panel C assumes $\tilde{V}$ for $Si_{80}Ge_{20}$, which has not been measured, is same as that measured for $Si_{89}Ge_{11}$. If the mechanism is B-Ge pairing then we might expect any Ge effect to saturate once the Ge concentration exceeded the B concentration.

[76] Y. Zhao, M. J. Aziz, N. R. Zangenberg, and A. Nylandsted Larsen, Appl. Phys. Lett. **86**, 141902 (2005).

[77] W. Windl (private communication).

[78] The scalar migration volume for each such combination would still be $+0.17\ \Omega$, the trace of Eq. (46).

[79] We cannot rule out the possibility of larger values of A arising from other ground-state saddle-point combinations.

[80] Y. A. Burenkov and S. P. Nikanorov, Sov. Phys. Solid State **16**, 963 (1975).

[81] S. P. Nickanorov and B. K. Kardashev, *Elasticity and Dislocation Inelasticity of Crystals* (Nauka Publishing House, Moscow, 1985).

[82] Y. Okada and Y. Tokumaru, J. Appl. Phys. **56**, 314 (1984).

[83] G. A. Slack and S. F. Bartram, J. Appl. Phys. **46**, 89 (1975).